Journal of Electroceramics 1:3, 239–272, 1997

Photochemistry of Nanostructured Materials for Energy Applications

BORIS LEVY

Boston University, Department of Chemistry, 590 Commonwealth Avenue, Boston, MA 02215

Abstract. A number of major disciplines have separately developed as distinct fields of energy research utilizing nanostructure materials: *i*. Heterogeneous photocatalysis; *ii*. Photoelectrochemistry—including electrochemical photovoltaic cells; *iii*. Photochemistry in zeolites and intercalated materials; *iv*. Photochemistry of thin films and membranes—including self assembled structures; and *v*. Supramolecular photochemistry. Photophysical properties of small particles, in the angstrom to nanosized regime—depending on specific material, resulting in band gap broadening as compared to bulk properties, and corresponding phenomena with organic dyes as a function of aggregate size having relevance to energy related applications are discussed, as are dielectric confinement effects controlling the geometric distribution of light absorption within a particle, aggregate or adsorbed molecular deposit. Synergism among fields has emerged, as for example with transition metal oxide photocatalysts and photoelectrodes, combined with supramolecular spectral sensitizing transition metal ligand complexes used to harvest light and vectorially transfer photo-generated electrons and holes along selected energetic pathways.

Two systems have already demonstrated potential for significantly reducing reliance on fossil fuels and concomitant environmental stress. These are: *i*. Pollution remediation with wide band gap semiconducting particulate and nanoporous photocatalysts; and *ii*. Electrochemical photovoltaic cells utilizing nanoporous semiconducting electrodes fabricated by lightly sintering nanosized TiO_2 particulates, followed by spectral sensitization with tri-nuclear ruthenium ligand dyes. Heterojunction contacts between inorganic photoconducting particulates, termed photocatalytic diodes, and three phase systems, termed photocatalytic transistors, have been demonstrated to increase photocatalytic conversion efficiency in catalytic processes and to increase light sensitivity of analogous silver halide photographic systems. Research being carried out in laboratories throughout the world, aimed at improving the efficiency and understanding of the multi-disciplinary processes involved are described. Suggested areas of investigation for achievement of short (∼5 years) and long term (5–20 years) goals are reviewed.

Keywords: photochemistry, solar energy conversion, nanostructured materials, pollution remediation, electrochemical, photovoltaic, spectral sensitization, heterojunctions, controlled-porosity, intercalation, supramolecules, zeolites, self assembly, mono- and multi-layers

1. Introduction

Solar energy falling on the 48 contiguous states each year amounts to about 1500X the yearly consumption of oil by American industry. This abundant supply of energy has the potential of providing photochemically based alternatives for fossil fuels. Nanostructured materials are being utilized in a variety of approaches demonstrating the feasibility of achieving this objective.

Areas of ongoing investigation include: harvesting of solar energy for direct conversion to electricity; production of alternative fuels; production of high value chemical products and precursors; pollution remediation; and development of light activated molecular level devices. Two of these photochemical processes, pollution remediation and electrochemical photovoltaic solar energy conversion, are sufficiently advanced to have excellent opportunities of making significant contributions toward reducing dependence on fossil fuel and resulting environmental stresses within the next five years.

Pollution remediation with wide band gap semiconducting particulate and nanoporous photocatalysts is at the present time a demonstrably viable process, capable of helping to address challenges such as the

cleanup of military, DOE and Superfund sites around the country, whose estimated cost is reported by Wilson [1] to be at about $650 billion. A wide range of organic pollutants in the air, water and soil have been mineralized at sufficiently high rates by heterogeneous photocatalytic processes to have justified commercial commitments by a number of industrial organizations. Recent accounts of progress in this area are given by Wilkins and Blake [2].

Progress in electrochemical photovoltaic energy conversion, using Grätzel Cell technology, has stimulated related research efforts by many university, government and industrial groups throughout the world. Prototype cells have been demonstrated to have high light absorption and energy conversion efficiencies, along with reasonable lifetimes, as described by Nazeeruddin et al. [3].

Both processes are at present based mainly on the use of nanocrystalline, particulate, aggregated, or lightly sintered porous coatings or packed pellets of TiO_2. Proposed methods for increasing efficiencies of photocatalytic and photovoltaic processes have been centered on a semiconductor device approach involving: *i*. Metal doping, *ii*. Mixed transition metal oxide formation, and *iii*. Heterojunction contacts with metallic surface deposits, inorganic semiconductors, sensitizing dyes and semiconductor/liquid junctions. Commercially available nanosized TiO_2 particles produced by Degussa as P-25 by ''fuming'' $TiCl_4$, has been widely used in laboratory investigations, process development and large scale feasibility studies. More recently, synthetic efforts have been directed toward sol-gel techniques for use in Grätzel Cell applications and for use in reactor designs for pollution remediation using porous TiO_2 in pellet form, as coatings on reactor walls or on other supports such as glass wool, etc. Here, controlled primary particle size and porosity of the aggregated and sintered composites are important factors that may require application specific optimization.

It is common to consider the following disciplines as distinct fields of energy related photochemical research: *i*. Heterogeneous photocatalysis; *ii*. Photoelectrochemistry—including electrochemical photovoltaic cells; *iii*. Photochemistry in zeolites and intercalated materials; *iv*. Photochemistry of thin films and membranes; and *v*. Supramolecular photochemistry. As will be evident, a welcome synergism has emerged among these categories, especially as they relate to the use of nanostructured transition metal oxide semiconductor photocatalysts combined with transition metal ligand complexes absorbing in the visible spectral region, to harvest light and vectorially transfer photo-generated electrons and holes along selected energetic pathways.

Photochemistry with nanometer sized materials ($\sim$1–100 nm) is the focus of this report. However, bulk materials, and particulates with dimensions $>$100 nm coupled with nano-dimensional deposits will also be discussed. Heterojunction structures offer special opportunities for vectorial direction of photocurrents and separation of charge carriers used to initiate chemical processes. Requirements for strict epitaxy between contacting semiconductor phases, in the sense applied in solid state devices, may often be relaxed when particle or layer thicknesses are sufficiently small, as has been discussed by Levy [4] and Tributsch [5]. Adsorbed organic and organometallic spectrally sensitizing dye monomers and aggregates on bulk or nano-dimensional materials are also considered to constitute nano-dimensioned systems. Self-assembled and derivitized surfaces of bulk and nano-dimensional particulate, thin film and membrane materials combined with small molecules and supramolecular species, as discussed by Balzani [6], are important areas of current research.

A number of excellent reviews emphasizing various aspects of this field, as defined above, have supplied useful reference material in our present needs assessment. See for example: [2] and [6–20]. (In addition, subsequent to the submission of the first draft of this Chapter (Nov. 1995), a report summarizing plenary lectures and panel discussions of a workshop sponsored by DOE/BES, ''Research Opportunities in Photochemical Sciences,'' (see [21]), has been made available on the internet.)

2. Solid State Device Approach to Heterogeneous Photocatalysis, Photoelectrochemistry and Pollution Remediation

Photoelectrochemical splitting of H_2O to form H_2 and O_2 by Fujishima and Honda [22] initiated a great deal of research activity, continuing to the present time. Single crystal TiO_2 electrodes combined with a Pt counter electrode were employed in these early investigations. Upward band bending in the *n*-type TiO_2 depletion layer at the solid/liquid interface was considered to provide a field for photoelectron drift

away from the surface upon which light was incident and for photohole drift toward this surface. When Beers Law applies, light absorption decreases exponentially with depth into the interior of the sample, measured from the surface upon which light is incident, resulting in charge carrier diffusion currents. With *n*-type materials, photoelectron diffusion is vectorially in the same direction as photoelectron drift, while photohole diffusion and drift are in opposite directions, as described by Bardeen [23]. The electrons reaching the electrical contact travel through the external circuit to the Pt electrode, where reduction of H^+ ions to H_2 occurs. Oxidation reactions leading to O_2 formation are initiated by photoholes at TiO_2 electrode, as shown in Fig. 1.

This work was followed by UV irradiation of aqueous suspensions of TiO_2, with both oxidation and reduction reactions leading to O_2 and H_2 evolution occurring on the same particle. Quantum efficiencies with both large single crystals and particulate suspensions were low, leading to speculation concerning the role of recombination of e^- and h^+. This led to experiments having as one aspect of their motivation an increase in mean charge carrier separation distance. Approaches employed, as reviewed by Serpone et al. [18] and by Kamat [12], include derivitized electrodes; particle size effects; spectral sensitization by adsorbed dyes; spectral sensitization by interparticle contact of broad band gap (i.e., TiO_2) and narrower band gap (i.e., CdS) particulate and colloidal suspensions. Metallic deposits (i.e., Pt, Rh, Au, Pd, etc.) on single crystal, particulate and colloidal broad band photoconductors have been used, where metal loading ranged from

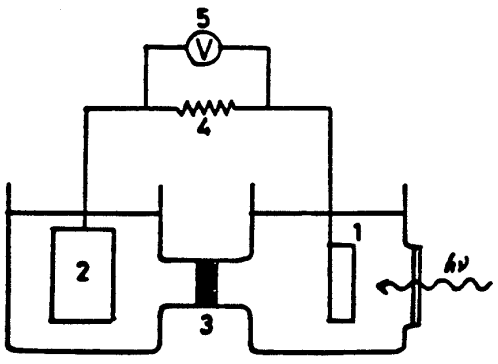

Fig. 1. Electrochemical cell in which the TiO_2 electrode (1) is connected with a platinum electrode (2), (3) is a fritted glass disc, (4) is a load resistor and (5) a voltmeter. From [22].

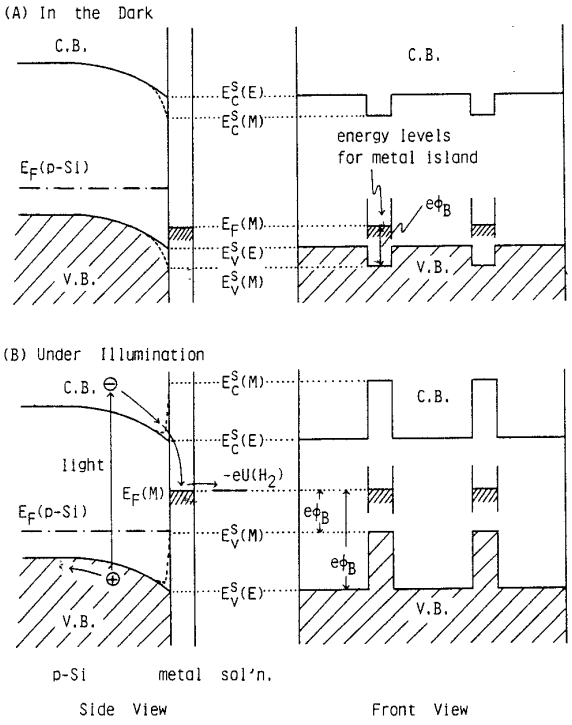

Fig. 2. Schematic energy band diagrams for a *p*-Si electrode coated with minute metal islands, in contact with 1.0 M HCl. E_F(*p*-Si) is the Fermi level for *p*-Si, and $U(H_2)$ the hydrogen evolution potential for the metal islands. Light excitation of the semiconductor injects photoelectrons into the metal islands, which raises the Fermi level of the metal to coincide with the $-eU(H_2)$. From [24].

trace amounts to ~10 wt.% In some instances very small metallic deposits, of only a few nanometer diameter, on a number of photoconducting substrates (i.e., Si, TiO_2, GaS, GaP, InP) have been observed by Nakato et al. [24] and [25] to display substantial improvements in quantum efficiency for H_2 evolution—an effect that was not specifically explained in the language of quantum size effects in current usage (see [19] and [7]), but which may constitute examples of this phenomenon, as illustrated in the energy band diagrams of Fig. 2.

2.1. Factors Relating Charge Carrier Transport Dynamics and Separation Distances to Chemical Kinetic Aspects of Photochemical Reaction Efficiency

Time resolved spectroscopic studies of photochemically initiated reactions at the surfaces of bulk,

particulate and colloidal photoconducting materials have been undertaken, in part, in an effort to understand the dynamics of charge carrier transport. When inclusion of reaction mixture additives or photocatalyst surface modification and/or doping coincide with the anticipated alteration in reaction rate or overall product yield, these observations have been interpreted by Heller et al. [26] on the basis of their presumed affect on recombination resulting from modification of the mean charge carrier separation distance.

Chemical kinetic and flash photolysis investigations by Heller et al. [26] and Grätzel [27] with colloidal photoconducting catalysts provide evidence that photo-initiated surface chemistry can occur in the picosecond to nanosecond time domains. Photophysical calculations predict little or no band bending at the surface of colloidal semiconductor materials having diameters smaller than the thickness of the space charge layer (i.e., >20 nm), as illustrated in Fig. 3. Transport times for charge carriers to reach the surface from the interior is estimated by Memming [14] to be of the order of 1 ps—a value much shorter than calculated recombination times, which are estimated to be >10 ns.

For larger particles of $\sim 1\ \mu$m, where band bending is expected, the estimated transit time for minority charge carriers to arrive at the surface is 10 ns. The arrival of photoholes at the surface of *n*-type materials

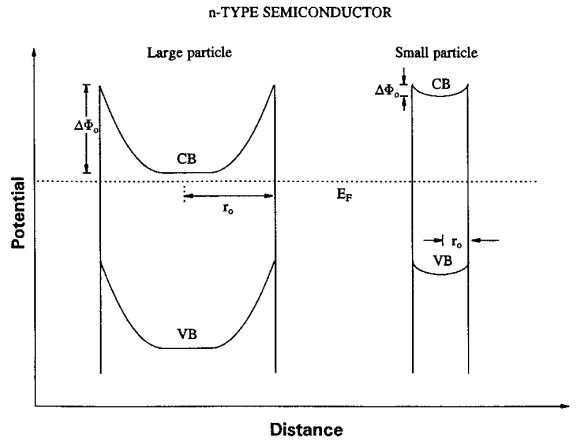

Fig. 3. Plots illustrating the formation of a space charge layer in a large and small semiconductor particle in equilibrium with a solution redox system, whose Fermi level is denoted E_F. Note that the small particle is nearly depleted of charge, the consequence of which is that its E_F is positioned at the middle of the band gap and the band bending is negligibly small. From [10].

and the population of the conduction band with photoelectrons will combine to flatten the energy bands, enabling photoelectron transport to the surface where recombination can compete with reactions of holes and electrons with adsorbed reactants. An analogous response will also occur in *p*-type materials, with depletion layers leading to downward band bending. The time for reaching flat band conditions has been estimated to be 30 ms, when the incident photon flux is 10^{17}.

Based on this analysis, it is reasonable to conclude that under stationary conditions of illumination (i.e., exposure times ≥ 30 ms) of single phase systems, with both small particles (~ 20 nm for Degussa P-25 TiO_2) and large particles ($\sim 1\ \mu$m and larger), the drift component of the driving force for charge carrier separation is essentially absent. Consequently, according to this picture, occurrence of low quantum yields with the larger particles and also with the colloidal catalysts, in the absence of a surface space charge, or externally applied field, may be largely the result of recombination.

With the 20 nm particles one would also expect relatively uniform light absorption across an individual particle. Therefore, unless there are other factors which are operational such as: *i*. Fields created by adsorbed reactants; *ii*. Dielectric confinement leading to non-uniform light absorption; and *iii*. Non-linear optical effects resulting from non-centrosymetric fields, as discussed in [7], [28], [29], both drift and concentration gradients leading to diffusion should be essentially absent and consequently one would expect minimal charge carrier separation. Under these sets of conditions, recombination should dominate.

Depletion and inversion layers and surface contact potentials can influence the magnitude and direction of photo-induced currents, as shown by Bardeen [23]. For isolated particles of sufficiently small diameter, surface band bending is not expected, as discussed in [14]. However, if the small particles are aggregated, the effective particle size may be in a size regime where band bending can be a factor influencing charge carrier transport.

Information concerning these parameters is accessible by application of time resolved photocharge techniques, TRPC, which is a measure of the dynamics of charge carrier separation and recombination, where the signal amplitude is proportional to the mean charge carrier separation distance and polarity of the signal provides information regarding the

distribution of absorbed quanta within the sample and the sign of the more mobile charge carrier. TRPC experiments indicate that continuous high intensity exposure collapses the depletion layer, if present, making it possible to obtain the intrinsic transport parameters characteristic of the photoconducting sample. Information regarding interfacial effects, due to adsorbed or epitaxial deposits, are also accessible by performing experiments with and without the CW high intensity exposure, thereby determining by difference the TRPC modulation by space charge and interfacial field effects. These measurements have been applied to silver halides and other photoconductors, including TiO_2; TiO_2/Pt and Pt/TiO_2/Dye, as shown by Zhang amd Levy [30]. The sample can be any photoconductor (single crystal, thin film, particulate solid, particulate or colloidal suspension or liquid).

Regardless of particle dimensions, heterojunction structures and especially multi-junction systems provide the possibility of spontaneous creation of a field across one the components during Fermi level equilibration, providing a significant driving force for charge carrier separation that might otherwise be absent. Considerations along these lines are among well accepted design criteria for fabrication of *p-i-n* thin film photovoltaic cells, as discussed by Takahasi and Konagai [31]. For this reason investigations of heterojunction catalytic systems of controlled composition, dopant concentration, and morphology, with dimensions that extend from the nanometer range into the micron and larger ranges are considered to be potentially fruitful areas of investigation. Similar considerations are also applicable in the field of silver halide imaging. For example, with silver halides of varying particle sizes (55–450 nm), it has been determined, by Zou et al. [32], that time resolved photocharge (TRPC) signals with the smallest particles could only be observed when they were sensitized with very small, nanosized or smaller, Ag_2S or AgAuS specs, as is common practice with commercial AgX imaging materials. After equilibration of Fermi levels with AgBr grains, the Ag_2S and AgAuS deposits have been shown to acquire positive space charges and function as trapping sites for photoelectrons generated by light absorption in the AgX.

The analysis discussed above encompasses the common presumption that the best way of minimizing electron-hole recombination is spacial separation. When the end products of a heterogeneous photocatalitic process do not depend on the interaction of intermediates formed by reaction of both holes and electrons, charge carrier separation over large distances may be advantageous (i.e., water splitting and photovoltaic applications). In other situations, as may sometimes be the case in the oxidative degradation of environmental pollutants, it may be important to reconsider the blanket endorsement of charge carrier separation as a means of enhancing reaction efficiency.

Illustrative of the importance generally assigned to charge carrier separation distance in explaining quantum efficiencies of photocatalytic processes is an investigation by Heller et al. [26], which focuses on the effects of pretreatment of particulate TiO_2. Reductive processes resulting in upward band bending of the TiO_2 was considered to promote charge carrier separation and reduce recombination at the surface, thereby enhancing photochemical quantum yields for the oxidation of 2-propanol. However, as plausible as this explanation may seem, it is difficult to completely reconcile it with the tendency for the system to move toward a flat band condition under constant intense illumination typical of many practical processes, since this removes or lowers the drift potential for photoelectron transport away from the surface, as seen in Fig. 4.

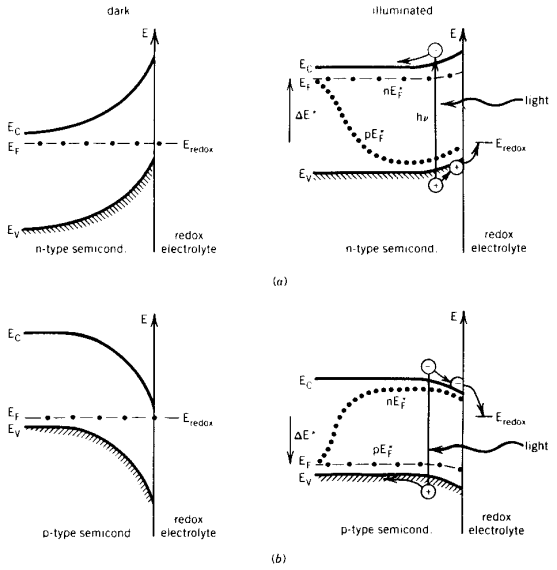

Fig. 4. Quasi-Fermi levels and photovoltages at an illuminated semiconductor-electrolyte contact with depletion layers. From [10].

A more recent account by Schwitzgebel et al. [33] of the photocatalyzed air oxidation of C_8 organics in contact with nanocrystalline *n*-TiO_2-coated glass microbubbles, provides a different view. Here, the overall reaction path leading to desired products involves interaction of chemical intermediates formed in both reduction and oxidation processes. Di-oxygen, O_2, plays a dual role: *i*. It reacts with conduction band electrons to form the superoxide radical ion O_2^-; and *ii*. It combines with organic radicals, $RR'CH\cdot$, generated by h^+ or ·OH radical reactions to produce organoperoxy radicals, $RR'CH(OO)\cdot$. It is further suggested that the superoxide migrates on the surface, or desorbs and migrates in solution—in either case eventually encountering and reacting with the organoperoxide radical on the surface to form an organotetroxide which decomposes in a reaction sequence similar to that occurring in Russell type reactions. Products formed are analogous to those shown in (1)

$$RR'CHOOOOH \rightarrow RR'CO + H_2O + O_2 \quad (1)$$

Upon introduction of the electron acceptor $FeCl_3$ to the reaction solution, a marked decrease in the yields of all of the final products of oxidation was observed and attributed to competition by O_2 and Fe^{3+} for photoelectrons [33]. This was regarded as strong support for the direct participation of both photoelectrons and photoholes in a Russell type oxidative degradation.

The role of Fe^{3+} has also been discussed by Bahnemann [34] for the photocatalyzed oxidation of dichloroacetic acid (DCA) using sol-gel prepared nanosized mixed, Ti and Fe oxides containing 0–50% Fe^{3+}. In Fig. 5 the quantum yields for H^+ formation, for reaction mixtures at pH 2.6 and 11.3, as a function of % Fe^{3+} content of the Ti/Fe mixed oxides are seen to go through maxima at 2.5% Fe^{3+} and 0.2% Fe^{3+}, respectively. Bahnemann attributes the increased degradation of DCA with increase in % Fe^{3+} to an increase in e_{cb}^--trapping by Fe^{3+}, which is assumed to decrease recombination. Further increase in % Fe beyond the observed maxima for DCA degradation is stated to increase recombination due to the decreasing number of Ti-surface states.

As a means of testing the widely held premise of a positive correlation between photo-induced charge carrier separation distance (CCSD) and the photocatalytic activity of particulate photocatalysts, Sadeghi et al. [35] have investigated the oxidative

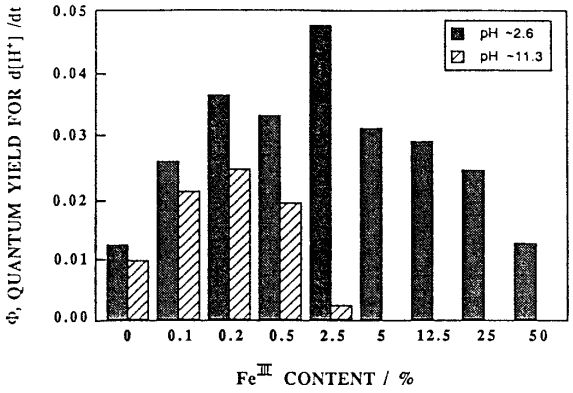

Fig. 5. Photochemical quantum yields for the formation of protons during the photocatalytic degradation of 2.5 mM dichloroacetic acid with Ti/Fe mixed oxide colloids of different iron content measured pH 2.6 and pH 11.3. From [34].

degradation of CH_3OH vapor in contact with coatings of particulate Pt(0–8 wt.%)/TiO_2 combined with time resolved photocharge (TRPC) measurements. Several commercially available co-fumed Fe_2O_3-TiO_2 (0, 2 and (6–8) wt.% Fe) particulate photocatalysts were also investigated. TRPC is capable of providing a non-contact electronically derived measure of CCSD, as described, by Levy [36]. Contrary to conventional wisdom, large CCSD values were found *not* to correspond with highest photocatalytic efficiency for the oxidative degradation of CH_3OH. Indeed the investigation of Sadeghi et al. [35] supports an extension of the ''Russell-like'' mechanism described in [33], in which photoelectrons e^- and photoholes, h^+, each initiate the formation of interacting chemical intermediates, i.e. $O_2^-\cdot$ and $HOCH_2(OO)\cdot$, in close proximity on the catalyst surface, thereby reducing the need for surface diffusion over large distances for the reaction to proceed toward production of the observed $HCOOCH_3$ intermediate. These chemical processes are believed to be competitive with charge carrier recombination at small CCSD values. It has also been speculated that the proposed extension of the ''Russell-like'' mechanism may provide an alternative explanation for the occurrence of a maximum degradation rate of aqueous solutions of dichloroacetic acid, using sol-gel prepared Fe_2O_3-TiO_2 mixed oxide photocatalysts as a function of weight % Fe, as described in Fig. 5. Intermediate levels of Fe^{3+} might trap photoelectrons and promote formation of $O_2^-\cdot$ at sites sufficiently close to those where the organoperoxy radical is formed, thereby increasing the probability of formation of the organotetroxide.

When the level of Fe^{3+} is high, photoelectrons trapped at Fe^{3+} sites may be expected to compete effectively for photoholes with reactions leading to organoperoxide, $RR'CH(OO)\cdot$, formation, thereby decreasing the overall degradation of DCA. At some intermediate Fe^{3+} level, observation of a maximum in degradation rate, as observed in [34] in mixed Ti/Fe^{3+} oxides, becomes plausible.

Gerisher [37], has referred to the importance of the rate of O_2 reduction by electrons in preventing recombination during photocatalytic processes utilizing semiconducting colloids and particulates. It is pointed out that O_2^- formaion may be the slowest step in the reaction sequence in the oxidation of organic molecules by ·OH radicals or directly by positive holes. Surface deposition of Pt or Pd clusters on TiO_2 has been demonstrated to accelerate O_2^- formation, thereby decreasing recombination and increasing product yields initiated by h^+ or ·OH. However, when the number and/or size of the metal clusters become too large, the advantages of metallic deposition are lost and these sites begin to function as recombination centers, as is also discussed in [35] and described in Figs. 6 and 7. When the metal cluster deposit acquires a size sufficient to display bulk metallic properties with work function well below that of the O_2 electron affinity, O_2^- formation by electron transfer from the large metal cluster to an O_2 molecule adsorbed to the TiO_2 surface becomes energetically unfavorable. Too high a number density of metal cluster deposits also favors recombination of photoelectrons trapped at metal clusters in close proximity to the sites of photo-induced electron-hole pair generation in the TiO_2 substrate.

The degradation of vaporized TCE and of CH_2Cl_2, in the absence of water vapor, in contact with P-25 TiO_2 has been observed by Lichtin and Avudaithai [38], to proceed with a photon efficiency close to 2 molecules degraded per absorbed quantum of light. This is also consistent with the observed dependence of the initial degradation rate on the photon flux kinetic order of 1 for both of these compounds. The explanation offered is that photoelectrons and photoholes independently follow separate pathways leading to degradation of the reactants with near 100% efficiency. If one accepts this scheme an implication is that recombination is either low or absent and that little can be gained by attempts to further optimize the charge carrier separation distance (CCSD) for these reactants with this catalyst. On the other hand, with

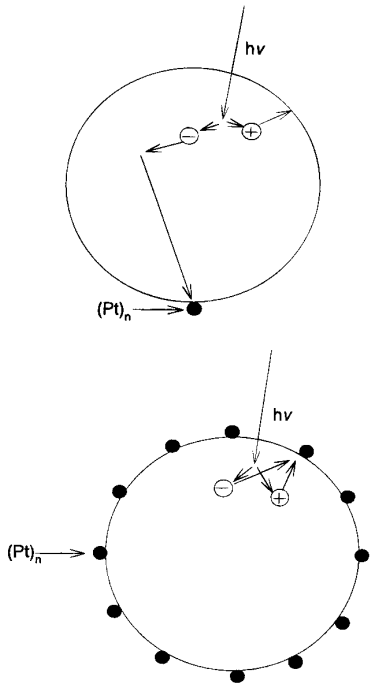

Fig. 6. Schematic diagrams showing the effect of number density of $(Pt)_n$ cluster deposits on TiO_2 in controlling charge carrier separation distance, CCSD: (a, top) low number density of $(Pt)_n$ deposits leading to increase in CCSD, as compared to TiO_2 in absence of Pt; (b, bottom) high number density of $(Pt)_n$ clusters leading to decrease in CCSD and increase in rate of charge carrier recombination. From [35], as adapted from [37].

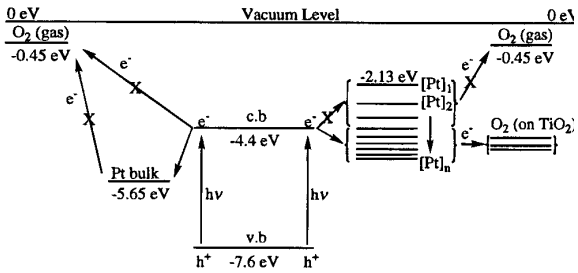

Fig. 7. Schematic diagram showing the positions of the top of the TiO_2 valence band and bottom of conduction band relative to the vacuum level = 0 eV, combined with (a) the relative position of the work function of bulk Pt within the band gap of the TiO_2; (b) the position of a single atom of Pt, based on electron affinity measurements, located above the bottom of the TiO_2 conduction band, and the range of available energy levels depending on $(Pt)_n$ cluster size and Fermi level equilibration of the Pt_n/TiO_2 heterojunctions; and (c) the position of the electron affinity of a gas phase O_2 molecule and the required stabilization for superoxide, $O_2^{\bullet -}$, formation when adsorbed to TiO_2. From [35].

dry CH_3OH vapor, the observed photon flux kinetic order is ~0.55, and the photoefficiency for degradation is 0.12 molecules/photon at an initial CH_3OH/O_2 ratio of 1%. Gerisher [37] has also discussed heterogeneous photocatalytic processes where a transition from linear dependence of yield on light intensity to a square root dependence is observed, with the linear dependence corresponding to a quantum yield close to one, and square root dependence for quantum yields below 0.3 if recombination predominates.

Raup and Dibble [39] and Lichtin et al. [40] and others have compared the relative efficiency for heterogeneous photocatalytic oxidative degradation of various organic pollutants with reactants supplied as vapors, or in the liquid phase. In a number of cases there appear to be higher efficiencies in the solid/vapor systems. Of related general interest, particularly when H_2O is present, is the role of the hydroxyl radical, ·OH, formed by reaction of h^+ with HO^-, and its subsequent reactions with organic species. A question which continues to be addressed is whether ·OH reacts on the photocatalyst surface with adsorbed organic species, or in the liquid phase with soluble organic molecules.

3. Optical Properties

3.1. Band Gap Broadening with Decreasing Particle Size of Inorganic Semiconductor Particles

Detailed knowledge of the optical properties of nanostructured materials is important to an understanding of the photophysical and photochemical processes that follow absorption of light quanta. Steigewald and Brus [19] use quantum mechanical molecular orbital calculations to explain quantum confinement effects on optical absorption, accounting for the now well established blue shift in the absorption spectra with decreasing particle size. Bawendi [7] has also provided a recent overview of this field.

As a means of explaining observed spectral shifts during the early stages of inorganic semiconductor particle growth, molecular orbital (MO), and linear combination of atomic orbitals coupled with molecular orbital (LCAO-MO) procedures provide information for the construction of energy level diagrams for clusters of several molecules up to sizes characteristic of the bulk semiconductor. Increasing the number of molecules in a cluster requires the addition of filled and empty orbitals to the energy manifold. This decreases energy differences between the filled orbitals, as well as the empty orbitals. The energy gap between the highest occupied molecular orbital (HOMO) and the lowest unoccupied molecular orbital (LUMO) is also observed to decrease. For a bulk semiconductor, the filled and empty states form separated continuums—i.e., the valence and conduction bands. In the Q-size regime, the energy levels within the filled and empty states remain discrete and the ''bandgap'' between the HOMO and the LUMO states increases, compared to the bulk material, as shown by Bahnemann in Fig. 8 [34]. These properties have led to applications in a wide range of fields—i.e., semiconducting quantum

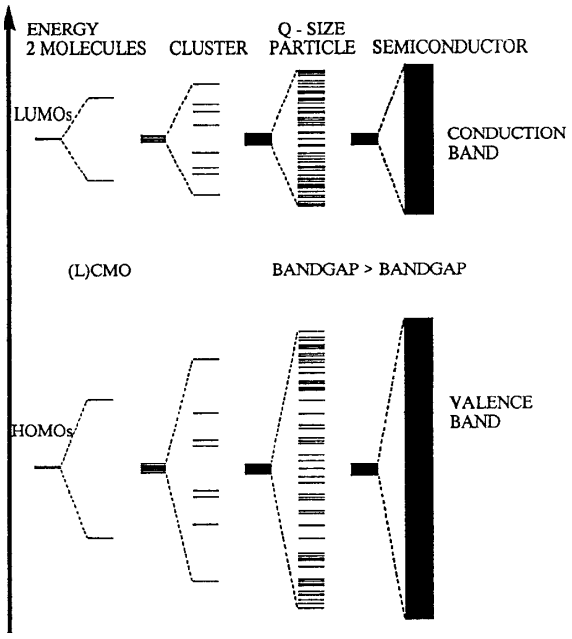

Fig. 8. Schematic diagram of the molecular orbital model for band structure. The number of available energy levels increases with increasing number of atoms in the cluster. This results in a decrease in spacing within the occupied and unoccupied levels and between the HOMO and LUMO levels. For bulk crystals the states within the occupied and unoccupied levels are sufficiently close to make it convenient to represent them as consisting of separated band structures, i.e., the valence and conduction bands. The energy gap between these bands is represented by the band gap, E_g, which increases in magnitude as the semiconductor particle radius decreases in size to the point where it becomes comparable or smaller than the exciton radius. From [34].

well and superlattice devices; non-linear optical materials; photocatalysis; and imaging systems. For II–VI compounds, maximum radii for the onset of quantum confinement effects (Q-size effects) leading to band gap increase have been determined by Bawendi [7] to be 10 to 100 Å. Wide band photoconductors such as TiO_2 (rutile) and ZnO undergo increases in band gap as the radii approach the range of 50 Å. It is interesting to note that a blue shift in the long wavelength optical absorption edge with decrease in particle size was first observed by Berry [41] for AgBr samples with radii of 65 Å and 350 Å.

3.2. Spectral Absorption Shifts due to Dye Aggregation

As discussed by Wang and Heron [29], molecular solids are viewed as possessing localized energy states with intermolecular bond energies which are much smaller than intramolecular interactions. Intermolecular interactions are considered only rarely to extend beyond nearest neighbors. This contributes to the frequently observed independence of the electronic properties (and presumably the spectral absorption properties) of molecular crystals with variation in crystal size, as distinct from band gap increases in Q-sized inorganic semiconducting materials.

However, contrary to the distinction made above between molecular aggregates and inorganic clusters, it is apparent that many of the more efficient silver halide spectrally sensitizing dyes fall outside of the generalized picture of molecular crystals and in many important respects posses aggregate size related spectral absorption characteristics in common with inorganic semiconducting Q-sized particles, as discussed by Levy et al. [42].

West [43] has reviewed the frequently observed hypsochromic (H-band) and bathochromic (J-band) spectral shifts of thiacarbocyanine dye aggregates in solution and adsorbed to AgBr grains with respect to monomer absorption in solution and in the adsorbed states—blue shifts correspond to H-bands and red shifts to J-bands. Spectral shifts to longer wavelengths for a benzothiacarbocyanine dye as a function of increasing solution concentration and also for increasing surface coverage on AgBr grains have been demonstrated by Levy and Mattucci [44], as seen in Fig. 9.

Considering the AgX/Dye system as a solid state heterojunction functioning as a photographic diode, spectral sensitization of silver halide grains by J-aggregates constitutes sensitization of the AgBr by Q-sized dye clusters, with the spectral region sensitized by the dye controlled by narrowing of the dye J-aggregate ''band gap'' with increase in aggregate size. This is analogous to bandgap increases with decreasing particle size of the Q-sized inorganic semiconductors. Both the Q-sized dye clusters and the Q-sized inorganic clusters have photoconducting properties, although by definition neither system has a band structure in the more traditional sense of bulk semiconductors, as discussed by Steigewald and Brus [19]. The mechanisms of photoconduction in these organic and inorganic systems may differ, but this should have no bearing on the ability of dye aggregates to display size dependent properties, i.e., Q-size effects, capable of causing shifts in absorptive and photoconductive properties. Indeed, LCAO-MO quantum mechanical calculations by Norland et al. [45] have been successful in predicting an $(N-1)/N$ dependence of spectral absorption shifts with sensitizing dye aggregate size, where N is the number of monomer units in the aggregate—with H-aggregates providing an increase and J-aggregates a decrease in band gap with increase in N, as reviewed by West [43].

3.3. Influence of Dielectric Confinement on Anisotropic Optical Absorption

It has been demonstrated experimentally and confirmed theoretically, that as a result of dielectric confinement light intensity at the back surface of a sample can be higher than at the front surface upon which light is incident. When this occurs photo-induced charge carrier diffusion currents are observed to flow in the direction vectorially opposing the incoming direction of the incident light. The phenomenon is a consequence of constructive interference of the incident and reflected light at the back surface and destructive interference at the front surface and is dependent on: *i*. Refractive indices of the sample and the surrounding media; *ii*. Sample dimension; *iii*. Sample absorption spectrum; and *iv*. Wavelength of the incident light, as has been shown in

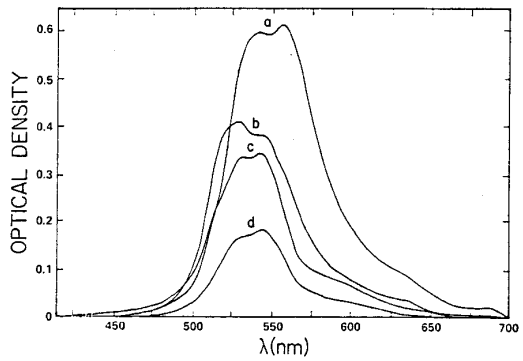

Aqueous solution spectra of dye D, 25°C.

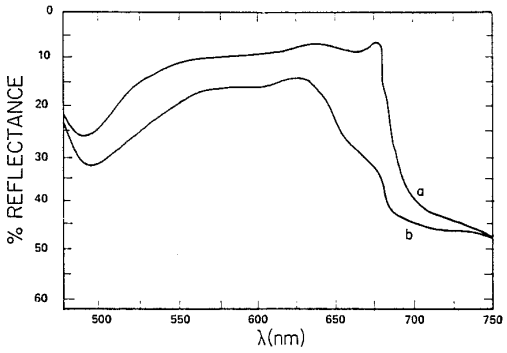

Reflectance spectra of dye D on AgBr

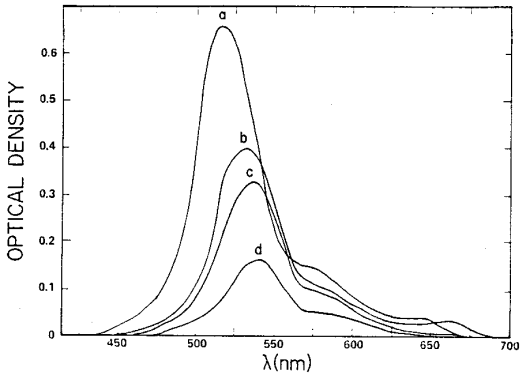

Aqueous solution spectra of dye E, 25°C.

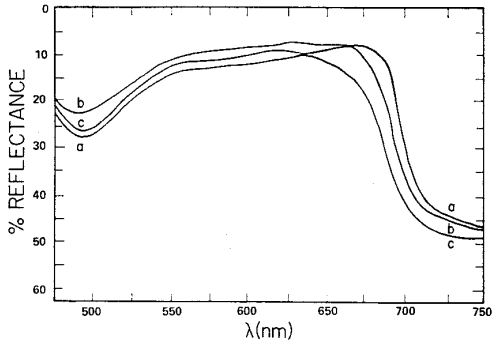

Reflectance spectra of dye E on AgBr

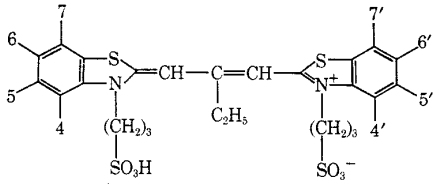

Dye D 6, 7 and 6′, 7′ =

Dye E 4, 5 and 4′, 5′ =

Fig. 9. Aqueous solution spectra of dyes D and E at 25°C: (a) 10^{-4} M; (b) 5×10^{-5} M (OD = chart OD × 1.25); (c) 10^{-5} M (OD = chart OD × 0.2); and (d) 5×10^{-6} M (OD = chart OD × 0.2). Increasing dye concentrations display increasing levels of J- and H-band molecular aggregation for dye D and E, respectively. Reflectance spectra of dyes D and E on AgBr at known surface coverages, as determined from Langmuir adsorption isotherms. For example with dye E surface coverages are (a) 4.96×10^{-6} M/m^2; (b) 3.12×10^{-6} M/m^2; and (c) 2.76×10^{-6} M/m^2. The J aggregate size increases in number of monomer units in the aggregate as the surface concentration of dye increases, as evidenced by the increasing red shift in the absorption at the higher coverages, following predictions of Norland, Ames and Taylor (1970). From [44].

[36], [28] and [29]. An example is the formation of $(Ag)_n$ clusters on the back surface of silver halide grains by exposure to light. These optically formed and oriented AgX/$(Ag)_n$, particulate heterojunction arrays were shown to be capable of time resolved photocharge (TRPC) polarity modulation by variation of light intensity of the laser probe pulse used in the measurement. This modulation is not displayed by

AgX particles in the absence of optically formed $(Ag)_n$ clusters. The mechanism of the TRPC modulation was shown by Zhang and Levy [46] to be dependent on the interfacial space charge and on dielectric confinement phenomena. This study has implications in the functioning of particulate photocatalysts in terms of the interaction of dielectric confinement on inhomogeneous light absorption, and on the manner in which interfacial field effects can control the vectorial direction of photocurrents, as modulated by light intensity.

4. Photochemistry of Particulate Photoconducting Materials

4.1. Silver Halide Imaging Materials

Spectral sensitization of silver halides by adsorbed organic dyes originated with Vogel [47] and has become an essential component of photographic imaging, although mechanistic investigations continue up to the present time. Nanosized silver bromide image recording materials, with an estimated grain size of 10–30 nm diameter, date back to the work of Lippmann [48] on color recording by use of light interference techniques to create standing-wave fringe patterns characteristic of the color of the object being recorded. This work has been viewed as an early example of holographic color imaging.

In an effort to form a clearer insight into those factors critical to efficient spectral sensitization by organic dyes, investigations utilizing inorganic elemental and compound photoconductor deposits from groups IV, II–VI and III–V to spectrally sensitize silver halide grains were undertaken in the late 1960s. This work led to the photographic diode mechanism of spectral sensitization. When combined with a third component, such as a spectrally sensitizing dye, the resulting amplification of the photographic sensitivity and photoconductivity led to the formulation of the photographic transistor mechanism, as reviewed by Levy [49]. Subsequently, it was realized that the dramatic increases in photographic sensitivity in the intrinsic region of silver halide light absorption, provided by small, later shown to be nanosize, epitaxial deposits of Ag_2S and AgAuS on AgX, where $X = Cl^-$, Br^- of I^- constitutes an important class of photographic diodes, which combined with an appropriate spectrally sensitizing dye, form photographic transistors [4]. Efforts to vectorially direct photocurrents to specific locations, as confirmed by TRPC measurements, either within or on the surface of individual grains which have been modified to form heterojunctions, have been successful in increasing photographic sensitivity to levels displayed by modern high speed commercial photographic films. Contributing significantly to this success has been the synthesis of AgX grains having distinct specially designed morphologies i.e. *i*. ''T'' grains consisting of thin tabular grains of Kodak, where the aspect ratio of grain ''diameter''/thickness is frequently 100/1, which clearly places these materials within the nanosized range for typical particle ''diameters'' in the 1–10 μm range; *ii*. The ''Double Structure'' grains of Fuji, and *iii*. The ''Multi-Structure'' grains of Konica. Also of interest is the work of Maskasky [50], and of Sugimoto and Miyake [51], dealing with small epitaxial AgX deposits on the surface of larger μm range grains of differing halide content.

4.2. Photocatalytic Heterojunctions Systems

Utilization of particulate photoconductors as photochemical catalysts appears to have been following a similar evolution as silver halide imaging (see for example [17]). Early work of Fujishima and Honda [22] utilizing UV irradiation of TiO_2 in water splitting, was followed by dye sensitization of photoconducting colloids and particulates derivitized in various ways to form photocatalytic heterojunctions, as described in [52–57].

4.2.1. Particulate photocatalytic heterojunctions. There has been considerable interest in the use particulate heterojunctions for the production of H_2 and O_2 from H_2O, as reviewed by Sakata [56] and also in the photocatalytic remediation of pollutants in air and liquids, as reviewed by Wilkins and Blake [2]. When employing particulate catalysts, consideration has been given to the separation of reaction intermediates and final products to avoid back reactions. To circumvent this problem reactants whose oxidation products are thermodynamically less likely to undergo back reaction with H_2 and which are more easily oxidized than H_2O have been employed. One approach uses particulate CdS mixed with TiO_2/0.5% RuO_2 suspended in an aqueous alkaline solution of H_2S. H_2 yields are significantly higher in the presence of the mixed catalyst system, as

compared to reactions carried out in the presence of either CdS or TiO_2/0.5% RuO_2 separately. A suggested mechanism by Serpone et al. [57] is the generation of a vectorial photoelectron current, originating from band gap excitation of each of these photoconducting materials, into the RuO_2 via the TiO_2 conduction band. Photohole transfer to the CdS surface is via the CdS and TiO_2 valence bands. It is further considered that the RuO_2 deposits serve as traps for the photoelectrons, decreasing the likelihood of recombination and allowing time for the degradation of H_2S to H_2 and S to proceed.

Experimental investigations of a series of related systems comprising CdS supported on SiO_2 particles together with Pt deposits on TiO_2, ZnO, SnO_2, or WO_3, each supported separately on SiO_2 particles, has been interpreted by Sobcyznski et al. [58] to function via band gap excitation of the CdS/SiO_2 followed by direct transfer to the Pt, in preference to transfer from the CdS conduction band to the TiO_2 conduction band from which electrons are injected into the Pt.

Another system of interest described by Parmon and Zamaraev [59] is the p-Cu_xS/n-$Zn_yCd_{(1-y)}S$/Pt heterojunction photocatalyst, used to spectrally sensitize H_2 evolution from adsorbed H_2S supplied in aqueous solutions. It is considered that photoelectrons excited into the conduction band of the $Cu_xS/n-Zn_yCd_{(1-y)}S$ heterojunction are energetically positioned to be directed to the Pt deposit which serves as the site for H^+ ion reduction to H_2.

The Pd/TiO_2/Rhodamine-B photocatalyst has been shown by Parmon and Zamaraev to spectrally sensitize the mineralization of aqueous solutions of oxalic acid, producing a new long wavelength band in the action spectrum for H_2 production, compared to that obtained with Pd/TiO_2. H^+ reduction is considered to occur at the Pd deposits, which attract the photoelectrons originating in the dye and TiO_2 phases. Oxidation of the organic acid is initiated by photoholes excited in the TiO_2 and dye phases, which are transported to the dye surface [60].

4.2.2. Epitaxial and quantum size photocatalytic heterojunctions. Gerisher and Lubke [61] and Spanhel et al. [62] have studied the CdS/TiO_2 system, consisting of thin, quantum sized CdS deposits on a TiO_2 electrode, providing a demonstration of spectral sensitization of the photocurrent by CdS that has been compared to dye sensitization and is analogous to the photographic diodes described above in section 4.1. Cd clusters are reduced on the TiO_2 surface from $Cd(NO_3)_2$ solution and then converted to CdS by immersion in a sulfide solution. The onset of CdS spectral sensitization is shifted to higher energies as the size of the CdS deposit decreases to the quantum size domain. In colloidal samples prepared by wet chemical techniques for attachment of TiO_2 or ZnO colloids to quantum size Cd_3P_2, fluorescent quenching of the Cd_3P_2 emission by electron injection into TiO_2 or ZnO has been observed in [62]. Quantum broadening of the Cd_3P_2 band gap with decreasing particle diameter is suggested as the mechanism making electron injection into the ZnO possible. Henglein et al. [63] have studied the Ag_2S/AgI system using fluorescent techniques to investigate the effect of Ag_2S size ranging from bulk to quantum size. Quenching of the Ag_2S fluorescence by contact with AgI and the appearance of new fluorescent bands, associated with transitions within the AgI at wavelengths that increase with Ag_2S size, were observed. CdS nanoparticles, as described by Zhou et al. [64], have been partially converted to PbS by displacement of the Cd in Cd-S surface bonds—a technique similar to that used in the formation of silver halide core-shell converted grains by Davey and Knott [65] and others to follow (see [66]). The band gap of the resulting CdS-PbS narrows to that of the PbS as the Pb content of the particle increases. The spherically layered CdS/HgS/CdS quantum dot heterojunction system is the subject of an interesting series of papers dealing with their preparation, characterization and photobleaching, see Mews et al. [67] and references therein. Applications in photocatalysis have not as yet been reported.

''Sandwich colloids'', have been described by Fitzmaurice et al. [68], consisting of nanometer range TiO_2 aqueous colloids upon which AgI was deposited by rapid sequential addition of $AgNO_3$ and KI solutions. It is concluded that photoelectrons are injected from the AgI conduction band into the TiO_2 conduction band and that the TiO_2/AgI systems are not simple mixtures of the separate colloidal components. The overall mechanism is considered analogous to that of conventional semiconducting photoconductor heterojunction diodes, the major difference being that the usual requirements for strict epitaxy are relaxed. Other photocatalytic heterojunction structures have been investigated

using TiO_2 and ZnO combined with CdS and Cd_3P_2 [62]; ZnO/ZnS [69]; AgI/Ag_2S [63]; TiO_2/CdS and CdS/AgI [70]. In each of these systems emphasis is on the suppression of recombination by charge carrier separation. However, charge carrier separation distances are not directly measured, but are inferred from transient absorption spectra, or by measurements where the photoconductor is in contact with an electrode, which may provide a field across the electrode/photoconductor interface capable of influencing the magnitude and, in some situations, the vectorial direction of current flow.

In a paper by Bedja and Kamat [71], heterojunction ''sandwich'' systems, using the terminology in [68], are compared to the optical, photocatalytic and photoelectrochemical behavior of colloidal photoconducting systems which are completely encapsulated by a second photoconductor, designated as capped systems to distinguish them from sandwich (also referred to as coupled) systems. Figure 10 provides schematic diagrams of the coupled and capped systems. These systems are similar to ''converted'' and ''core-shell'' photographic systems, which have their origins in the internally sensitized emulsions described in [65] and [66].

Figure 10 compares the photoelectrochemical response of nanocrystalline semiconductor films of SnO_2 and TiO_2 in the so-called coupled and capped configurations coated on an optically transparent electrode (OTE). With the coupled system, the SnO_2 is in contact with the OTE and electrons generated in both the TiO_2 and SnO_2 can be injected into the OTE. As is apparent, the SnO_2 colloid encapsulated by TiO_2 is essentially incapable of transporting photoelectrons to the OTE electrode. Instead photoelectrons generated in the SnO_2 remain trapped within this phase, while photoelectrons originating in the TiO_2 phase are injected to the SnO_2 and are isolated from the OTE by the TiO_2 capping deposit. Though not stated in the paper, it appears likely that a SnO_2 colloid capped with TiO_2 would be of limited utility as a photocatalyst under CW illumination due the trapping of photoelectrons in the capped SnO_2 phase, which would most likely lead to large recombination losses.

Lawless, Kapor, and Meisel [72], discuss the capping of CdS Q-sized particles formed by injection of saturated solutions of H_2S into deaerated solutions containing $CdClO_4$, hexametaphosphate and a bifunctional mercaptocaboxylic acid (HS- $(CH_2)_n$-CO_2H, $n = 1$–3). Stabilization of the CdS particle

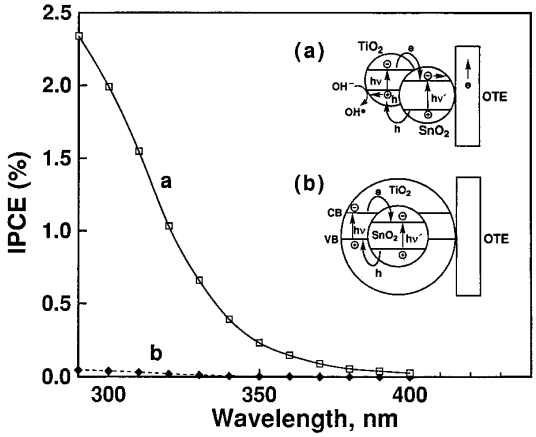

Fig. 10. Incident photon current efficiency (IPCE) versus light excitation wavelength for photoelectrochemical cells with sandwich structure and capped structure electrodes: (a) TiO_2/SnO_2 sandwich structure; and (b) TiO_2/SnO_2/TiO_2 capped structure. In capped structure photoelectrons are directed from the TiO_2 conduction band to the interior SnO_2 core, making them unavailable for collection by the optically transparent electrode (OTE). From [71].

size is through the HS-group of the bifunctional acid, which is added to the solution prior to the H_2S. The solution containing the capped CdS particles is purged of excess H_2S prior to addition of TiO_2 particles of 6.6 nm radii, which are bridged to the CdS particles through the carboxylic acid group (HS- $(CH_2)_n$-CO_2H) to form CdS-MPA-TiO_2 for the case where $n = 3$ and MPA = 3-mercaptopropionic acid. Emission spectra obtained with samples containing TiO_2 bridged to the capped CdS particles suggests quenching of blue emission associated with the capped CdS due to electron transfer to the TiO_2.

Other areas of extensive investigation include particulate semiconductor catalysts with metallic surface deposits (i.e., Si, InP, GaP, TiO_2) for promotion of chemical reactions, as reviewed in [55] and [73]. Photocatalytic activity was interpreted in terms of energy band diagrams, explaining advantages of discontinuous nano-sized metallic deposits of Pt, Pd, etc. (see Fig. 2 and [24,25]).

Choi et al. [74] have correlated the photoreactivity and transient absorption recombination dynamics of quantum sized TiO_2 colloids doped with 21 different metal ions at levels of 0.1–0.5 atomic %. Doping with Fe^{3+}, Mo^{5+}, Ru^{3+}, Os^{3+}, Re^{5+}, V^{4+}, and Rh^{3+} increases photoreactivity for oxidation and reduction reactions, while Co^{3+}, and Al^{3+} doping

decreases reactivity. The transient absorption studies are interpreted as displaying longer trapped photoelectron lifetime for photocatalysts having higher reactivity.

Martin et al. [75], following up on the work of Choi et al. [74], provide additional details on TiO_2 samples doped with 1% V^{4+}, and calcined at temperatures ranging from 25–800°C. Calcining temperature of the doped sample is correlated with quantum efficiency (ϕ) for rate of degradation of 4-chlorophenol. For all calcining temperatures, V-doping at 1% decreases ϕ, as compared to undoped TiO_2. At 600°C and 800°C, ϕ values for the doped samples are reported to be zero. Time resolved microwave photoconductivity (TRMC) signal magnitudes of samples calcined at 25, 400 and 800°C are also substantially decreased as a consequence of 1% V-doping-probably by a factor approximating 8, as judged by the reported laser energies of 38 mJ and 4.5 mJ required for observation of the TRMC signals for V-doped and undoped TiO_2 samples, respectively. Among the doped samples, the 800°C calcined sample has the largest TRMC response, but decays most rapidly. The large decrease in magnitude of the TRMC response as a result of V-doping, which correlates with the decrease in ϕ for each of the doped samples, is of special significance (*in the opinion of the author of this chapter*). Since TRMC signals are primarily a measure of the time resolved concentration of photoelectrons in the conduction band (see for example the early work of Kellogg [76]), the difference in signal magnitude between doped and undoped TiO_2 may reflect a more rapid recombination of photoelectrons with holes in the doped samples, which is also expected to correlate with ϕ.

4.2.3. Porous photocatalysts. Brief mention is made here concerning the use of porous TiO_2 for heterogeneous photocatalysis. Anderson et al. [77] have used sol-gel techniques in the preparation of porous TiO_2 pellets for use in packed reactors with excellent results for TCE mineralization. Sol-gel techniques of a similar nature have been adapted by O'Regan and Grätzel [78] in the formulation of nanocrystalline electrodes for electrochemical photovoltaic cells, as will be discussed in more detail below. Pelizzetti et al. [79] have compared the effects of variation of porous TiO_2 pellet diameter with photocatalytic efficiencies. Lichtin and Avudiathia [80] use a water slurry to coat their reactor walls with P-25, which also produces a porous coating.

Yasumori et al. [81] and Anderson and Bard [82] have described the catalytic activity of sol-gel preparations of SiO_2-TiO_2 mixed oxides. Yasumori et al. [81] platinized the TiO_2 sol and combined it with a SiO_2 sol prior to gelation. The mixed oxide was found to be 4X more active as a photocatalyst for hydrogen production from ethanol than the Pt/TiO_2 alone. Anderson and Bard [82] found their mixed oxide preparation for the photocatalyzed decomposition of rhodamine-6G to be 3X more active than Degussa P-25. Photocatalytic activity was shown to correlate with the saturated surface coverage of rhodamine-6G on the mixed catalyst, which tended to increase with increasing % SiO_2. SiO_2 alone was found to have no photocatalytic activity.

5. Photoelectrochemistry

5.1. Electron Transfer Across the Semiconductor/Liquid Electrolyte Interface

Nozic [15] has discussed possible advantages of superlattice photoelectrodes in contact with solution as a means of achieving ''hot'' electron transfer across the semiconductor/liquid electrolyte interface. Photo-induced charge carriers generated within the quantum wells are confined by the energy barriers imposed by the large band gap component of the supperlattice and by the energy barrier for charge transport imposed by the solution. Quantization of photoelectron energy states in the quantum wells extends their life-time in the high energy states, as compared to rapid cooling of high energy electrons to the bottom of the conduction band, as occurs with bulk semiconductors. This provides the opportunity for ''hot'' electron transfer to redox acceptors in solution that would be energetically inaccessible to electrons at the bottom of the conduction band of bulk semiconductors. Avoidance of heat losses in this manner has the potential of significantly increasing solar energy conversion efficiency. Quantitative evaluations of competitive rates of cooling versus injection in supperlattice photoelectrochemistry represent major unresolved experimental and theoretical issues which are being actively studied and debated, see for example [16], and [83–86].

In device grade GaAs(100) electronic relaxation

has been observed by Bromer et al. [83] to be 10–50 femtoseconds for electrons >0.3 eV above the bottom of the conduction band. Electron cooling dynamics are found to be nearly an order of magnitude slower for molecular beam epitaxy (MBE) grown GaAs, suggesting that it may be possible to control electron cooling rates in the MBE materials by controlled removal of surface defects. Ferrocene redox couples appear to be optimally poised acceptors for hot electrons from MBE grown GaAs electrodes, in support of the concept of ''hot'' electron transfer.

5.2. *Nanoporous Photoelectrode Materials*

Porous nanocrystalline semiconductor thin films are rapidly coming into the forefront as a new class of materials for catalysis and photocatalysis, due to their unusual optical and electronic properties. The past decade has witnessed the development of several new types of electrochemical and chemico-electronic devices based on colloidal transition metal oxide films, such as the ''Grätzel'' liquid junction photovoltaic cell described by Nazeeruddin et al. [3], electrochemical electrochromic devices, Hagfeldt et al. [87], and solid state sensors of Lin et al. [88]. The afore-mentioned examples are distinguished from their compact-film counterparts by their superior performance, with a capability of absorbing approximately 90% of the visible incident light and displaying an over-all photovoltaic conversion efficiency under diffuse daylight of 11–12% using the configuration in Fig. 11. The electronic properties of these materials are largely derived from the enhanced surface area, as the role of localized states in electronic conductivity is greatly exaggerated in comparison to compact films. In addition, some size quantization effects are evident as shown in [90] and [91]. Dielectric confinement effects have been observed [28], [29], which control the regions of highest light absorption within individual particles or aggregates and concomitantly the vectorial directions of photo-induced charge carrier transport, also apply to nanoporous TiO_2 materials [42], [92].

Nanostructured TiO_2 comprises a contiguous network of lightly sintered colloidal particles and aggregates, generally with primary particle size 1–20 nm in diameter, accompanied by a substantial void volume (50%), giving rise to the extremely high surface to volume ratio, and porosity. Concerning the latter, the pores are interconnected, with pore

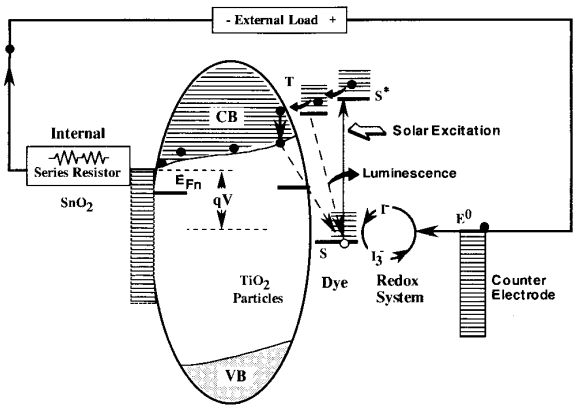

Fig. 11. Energy band diagram of Grätzel cell showing electron injection from the excited dye, and loss mechanisms. From [89].

diameters on the order of several nanometers. The films are usually structurally sound, and are attached to conducting substrates. Generally, degenerately F-doped SnO_2 films on glass sheets are used if transparent electrodes are desired. In the case of transition metal oxide colloidal films, the materials are not intentionally doped, and exhibit very large resistivities at normal temperatures ($\sim 10^{12}\,\Omega$-cm) in air, as observed by [93].

Due to the complex structure of nanocrystalline oxide films, attempts to model underlying conduction mechanisms based on a detailed knowledge of the internal electric field structure have been impeded. It is not possible to use standard models based on compact materials. However, this difficulty has been circumvented to some extent by the advancement of simple models that explain experimentally observed results with relatively good success. Specifically, transient electrochemically derived photocurrents have been simulated using a trap-filling and -emptying model based on Shockley-Read-Hall kinetics. It was shown in the model of Schwarzburg and Willig [94], that deep traps can control the rise and decay time constants of the transients, and that a wide distribution of traps was needed in the simulations to adequately mimic the experimental curves. Convincing experimental evidence of Könenkamp et al. [95], indicating that traps are operative in colloidal films, include measurements of slow non-exponential photocurrent decay which depends on the applied reverse bias. Several other related studies of note are cited [96–98].

The electric field distribution in colloidal oxide films is not known. However, calculations predict that

undoped individual particles are smaller than the Debye screening length known for the bulk material, thus precluding intra-particle band-bending [3]. In addition, the drift length of electrons in solid state diode devices under reverse bias, have been estimated to be on the order of 100 nm (particle sizes in these films are typically 20 nm) [95]. Thus, it is apparently clusters of particles that support the electric fields for which TRPC measurements provide evidence.

In a recent experimental study, results are presented demonstrating the existence of a built-in contact potential in the form of downward band-bending from the TiO_2 to the SnO_2, at the SnO_2/TiO_2 junction [42]. When a tri-nuclear Ru ligand dye, $Ru(II)(L)_2(CNS)_2$, closely related to the molecule suggested by Amadelli et al. [99], and discussed below, is added to this system, to form the SnO_2/TiO_2 (nanoporous)/Dye device, it is considered to fall within the *quantum well* class of devices discussed by Bube [100], if one includes a self biasing feature common in *p-i-n* photovoltaic cells. Here TRPC measurements described in [4], are used for the first time to detect the presence of a built in field, shedding some in-sight into the electric field distribution in nanoporous TiO_2 films. A proposed energy band diagram for a combined *p-i-n + quantum well* device, that is consistent with the structural configuration of the electrode and the TRPC measurements, is given in Fig. 12.

In a detailed description of the ''Grätzel cell,'' Nazeeruddin et al. [3], describe the spectral sensitization of nanocrystalline TiO_2 electrodes by imbibition in 3×10^{-4} M ethanol solutions of *cis*-X_2Bis(2,2′-bipyridyl-4,4′-dicarboxylate)ruthenium(II) charge-transfer sensitizers ($X = Cl^-$, Br^-, I^-, CN^-, and SCN^-) for 3 hours, followed by extraction from the dye solution and drying in a dry air stream. This is stated to result in monolayer coverage of the available TiO_2 surface. However, in the same paper it is also pointed out that under some conditions, not all of the nanoporous TiO_2 surface is available for coverage by the $RuL_2(NCS)_2$ dye. This may be due to nanosized pore diameters, which in some regions may be comparable or smaller than the dimensions of the dye molecule (or dye aggregate). Scanning electron micrographs of cross sections of these electrodes confirm their nanoporous structure over most of the TiO_2, with a denser less porous region at the SnO_2/TiO_2 interface, as shown in [3]. It is also found that during operation of the cell, the distribution of the $RuL_2(NCS)_2$ dye on the TiO_2 surface, ''accumulate(s) in certain zones while others are depleted.'' This is accompanied by a decreased incident photon-to-current conversion efficiency (IPCE). If net light absorption remains unaltered during dye redistribution, this suggests that charge injection by multi-layer dye deposits are less efficient in sensitizing TiO_2 then are monolayer Ru-ligand dye deposits attached

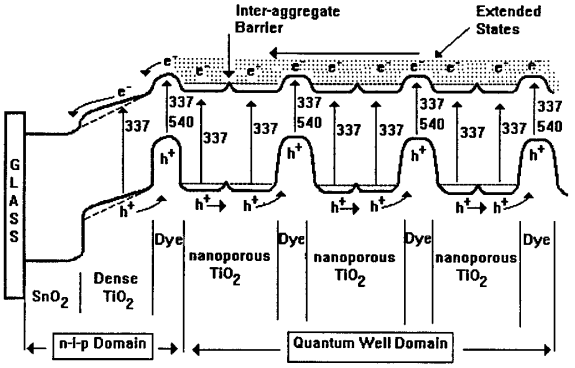

Fig. 12. Proposed energy band diagram for a *p-i-n + quantum well* Grätzel cell electrode consisting of dye sensitized nanoporous TiO_2 coated on heavily F doped transparent SnO_2. The spectral sensitizer is the tri-nuclear ruthenium antenna dye containing -CNS- groups in place of the -CN- groups of Fig. 17(a). The band structure of the electrode is based on the results of TRPC measurements with excitation by either a 337 nm laser pulse or a 540 nm laser pulse, both with and without CW illumination by a xenon lamp. Sample exposure is through the transparent SnO_2(F) electron, and in separate experiments with reversed sample orientation with respect to the surface upon which the light was incident. Photoelectron current for both orientations and for 337 nm and 540 nm excitation, was toward the SnO_2(F) electrode—this is dramatically seen as a reversal of TRPC signal polarity with reversal in sample orientation with respect to the light source. With non-spectrally sensitized samples TRPC signal polarity reversals are not obtained—photoelectrons move vectorially in the same direction as the incoming direction of the incident light. Similarly, in the absence of SnO_2 (F), with or without spectrally sensitizing dye, sign reversals are not observed. From these measurements it is concluded there is a *n-i-p* region, where the dye is physically blocked from symmetrically coating the nanoporous TiO_2, creating a field across the TiO_2 capable of directing photocurrents toward the strongly *n-type* SnO_2(F). In the region of the electrode removed from the SnO_2(F)/TiO_2 interface, the structure can best be represented by $[/(Dye)_m\ /(TiO_2)_n]_Q(Dye)_m$, where m = number of monomer units in dye aggregate, n = number of particles in TiO_2 aggregate and q = number repeating $/(Dye)_m/(TiO_2)_n$ units in electrode cross section. TiO_2 quantum wells created by symetrically adsorbed dye aggregates lead to the population of extended states in the $[/(Dye)_m/(TiO_2)_n]_Q(Dye)_m$ region of the electrode. Charge carriers in this region have been shown by TRPC measurements to be capable of being sensed by the field in the *n-i-p* region of the electrode, leading to attraction of photoelectrons generated in this quantum well region toward the SnO_2(F) electrode. From [92].

directly to the TiO_2. (Similar dye coverage dependent efficiencies are commonly observed in silver halide dye sensitization.) Recent absorption spectra of $Ru(II)(L)_2(CNS)_2$ in ethanol solutions ($3 \times 10^{-6} - 3 \times 10^{-4}$ M) by Sadeghi [101], and Raman spectra of nanoporous TiO_2 spectrally sensitized by $Ru(II)(L)_2(CNS)_2$, reported in [102], reveal the presence of dye aggregates.

Analogous photovoltaic results have been reported for porous films of wide band gap photoconductors spectrally sensitized by deposits of quantum sized inorganic photoconductors of band gap smaller than that of the porous substrate. A modified of O'Reagan and Grätzel [78] procedure for preparation of porous nanocrystalline metal oxide films of TiO_2, ZnO, SnO_2, Nb_2O_5 and Ta_2O_5 on conducting glass has been described by Vogel et al. [103], and employed as the substrate into which quantum size PbS, CdS, Ag_2S etc. were deposited within the pores, having sizes controlled by pore diameter, with correspondingly controlled band edges for spectral sensitization of the photocurrent in photoelectrochemical measurements. Techniques for improvement of the photostability of the electrodes are presented.

6. Molecular Level Light Harvesting and Energy Conversion

Baxter et al. [104] have identified the following molecular level approaches to artificial photosynthesis: *i*. Giant (supramolecular) molecules, in which the desired components are assembled by linear synthesis; *ii*. Peptide assemblies—in which amino acids are linked to form peptides with controlled spatial composition; *iii*. Microstructures in polymeric films; *iv*. Molecular assemblies on surfaces and interfaces; *v*. Membranes where there is a basis for assembling multiple components and *vi*. Soluble polymers with polymeric backbones capable of being derivitized with groups having desirable well established photophysical, electron transfer, or energy transfer properties. Molecular features considered essential to be present in the same structure include, ''...light absorption, spatially directed electron transfer by the utilization of free energy gradients, and the delivery of the photochemically produced oxidative and reductive equivalents to catalytic sites.'' It is further considered that it, ''...seems inevitable that in order for these features to be combined in a single molecular system will require a high level of molecular complexity.'' Representative examples of these types of systems are given below.

6.1. Giant Molecules

6.1.1. Approaches utilizing transition metal complexes. Transition metal complexes have been used to harvest visible light in energy conversion and storage applications designed to mimic the photosynthetic center in its ability to efficiently absorb light and to create and separate charge carriers for use in photovoltaic devices, or to initiate chemical reactions leading to energy storage through the production of high energy chemicals. Figures 13–16, from Serpone et al. [18], summarize important structural, spectral, photophysical, photochemical and energy and electron transfer features of $Ru(bpy)_3^{2+}$ ligands. These molecules, typical of many other mono-nuclear transition metal complexes, afford a basis for understanding the more complex supramolecular multinuclear metal complexes, which are the subject of great current interest. The approximate diameter of a sphere encompassing the $Ru(bpy)_3^{2+}$ molecule of Fig. 13, where bpy is 2,2′-bipyridine, is 1.4 nm. Figure 14 shows the low energy metal-to-ligand charge transfer, MLCT, absorption bands appearing in the visible spectral region, which are characteristic of these materials. The presence of the metal produces spin orbit coupling, helping to break down selection rules forbidding transitions between singlet and triplet ligand excited states. This allows light energy to rapidly cascade down to the lowest energy excited state with high quantum efficiency. Figure 15 gives a molecular orbital energy level diagram for a ruthenium(II) polypyridyl complex. Figure 16 shows possible energetic positions of the MLCT and the metal centered, MC, electron transition states, together with possible deactivation channels.

Serpone et al. [18] have also provided an excellent review of light-induced electron transfer reactions in the homogeneous and heterogeneous phases, including a discussion of the Marcus theory of electron transfer, which plays an ever increasing role in explaining the kinetics of these systems. Investigations in homogeneous systems continue to receive much attention. Applications to charge carrier separation and vectorially directed photocurrents involving transition metal ligands in combination

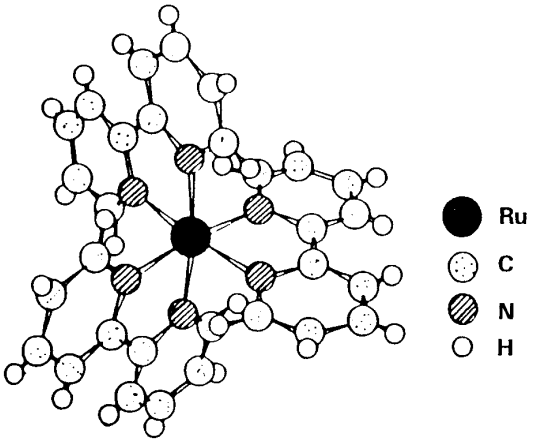

Fig. 13. Structure of a ruthenium(II) polypyridine complex: $Ru(byp)_3^{2+}$, where bpy is 2,2′-bipyridine. From [18].

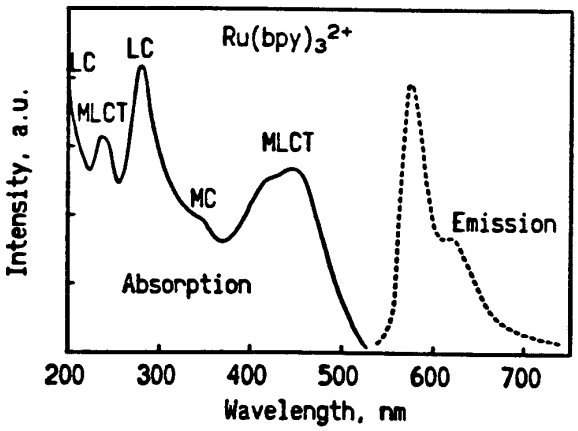

Fig. 14. Electronic absorption and emission spectra of $Ru(byp)_3^{2+}$ in aqueous and in ethanol/methanol, respectively at ambient temperature. From [18].

with a variety of donors and acceptors have been reviewed by Serpone et al. [18].

6.1.1.1. Tri-nuclear transition metal complexes—antenna systems. The tri-nuclear metal complex of Fig. 17a was synthesized and successfully tested by Amadelli et al. [99] for purposes of improving the light harvesting efficiency of the related mononuclear $Ru(bpy(COO)_2)_3^{4-}$ dye, used as a spectral sensitizer of nanoporous TiO_2. The light harvesting mechanism was considered to be the following:

$$S{\cdot}P\text{-}A + h\nu \rightarrow S{\cdot}P^{*}\text{-}A$$

$$S{\cdot}P\text{-}A + h\nu' \rightarrow S{\cdot}P\text{-}A^{*}$$

$$S{\cdot}P\text{-}A \rightarrow S{\cdot}P^{*}\text{-}A$$

$$S{\cdot}P^{*}\text{-}A \rightarrow S(e^{-}){\cdot}P^{+}\text{-}A$$

where, S is the TiO_2 surface; P is the central Ru-ligand unit attached to the TiO_2 through the COO^- groups in the dye; and A are the antenna Ru-ligands attached to the central unit through the -CN- groups.

Amadelli et al. [99] consider the following relationship, $h\nu' \geq h\nu$, an essential requirement for the molecule of Fig. 17a to function according to the energy level diagram shown in Fig. 17c. However, this energetic requirement may be too restrictive. For example, consider a hypothetical tri-nuclear molecule with antenna units consisting of metal ions, M^{2+}, where the M^{2+} to ligand charge transfer state, ^{1}MLCT, is at higher energy than the ^{1}MLCT state originating from the central metal ion, i.e. Ru^{2+}, to its ligands. In addition, the ^{3}MLCT state for M^{2+} should be at higher energy than the ^{3}MLCT state of Ru^{2+}. This might be accomplished if the ionization potential of $M^{2+} < Ru^{2+}$ and also by an appropriate selection of ligands, which could differ for each metal ion if

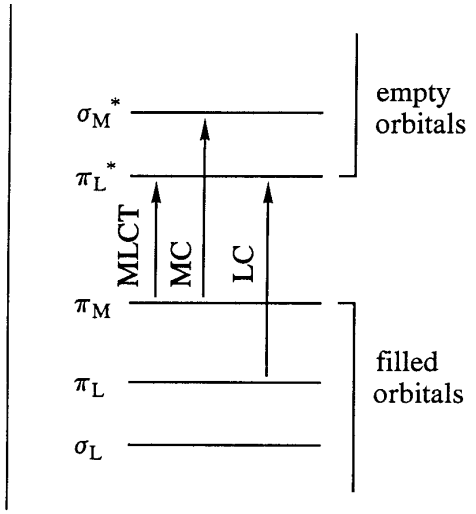

Fig. 15. Schematic representation of a molecular orbital energy level diagram for a ruthenium(II) polypyridyl complex, $Ru(NN)_3^{2+}$, in octahedral symmetry, illustrating the various possible electronic transitions: MLCT denotes an electron transition from an orbital predominately metal in character to one that is predominately ligand (metal-to-ligand charge-transfer); MC denotes metal centered electron transition in which the electron is simply redistributed amongst metal like orbitals; LC refers to ligand centered electron transitions in which electrons migrate between orbitals largely ligand in character. From [18].

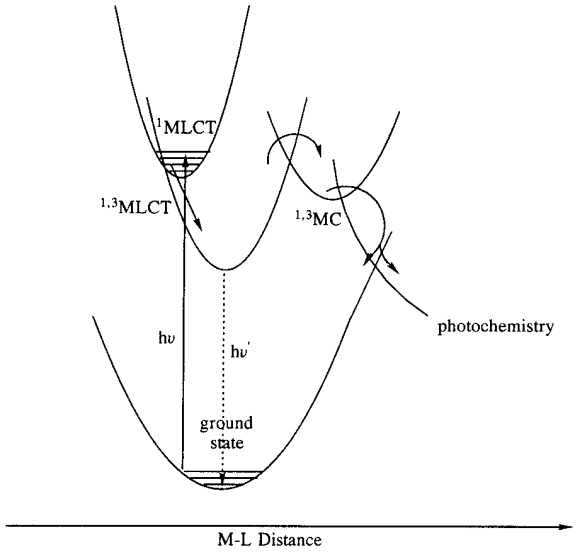

Fig. 16. Scheme showing the possible energetic positions of the MLCT and MC states in a complex like $Ru(byp)_3^{2+}$, together with the possible deactivation channels of the optical electron transition energy. From [18].

necessary. Under these circumstances, the energy relationship for excitation of the antenna ligands and the central Ru ligand may be reversed—namely, $h\nu' \leq h\nu$. This later relationship is the usual situation for spectral sensitization, where the goal is to extend the spectral response of the material being sensitized beyond its long wavelength absorption edge.

6.1.1.2. Multi-nuclear dendrite transition metal complexes. Serroni et al. [105] have described a synthetic method for the preparation of a supramolecular species having specific functions based on transition metal complexes. Neglecting counter ions, this molecule contains 22 ruthenium metal centers, 1090 atoms in total, has a molecular mass of 10,890 and an estimated size of 5 nm. Extension of the method to other metal ions and various ligands is considered straight forward. The synthesis is described as being based on a, ''protection/deprotection procedure in which a complex is used as a ligand and another is used as a metal...''. The reader is referred to the original paper for additional details. However, it should be kept in mind that the nanoporous TiO_2 electrode introduced by O'Regan and Grätzel [78] has already been stated to be incompletely covered by the tri-nuclear Ru(II) dyes (≈1.4 nm ''diameter'') described in [3], [78] and [99], probably due to the narrow pore dimensions of the

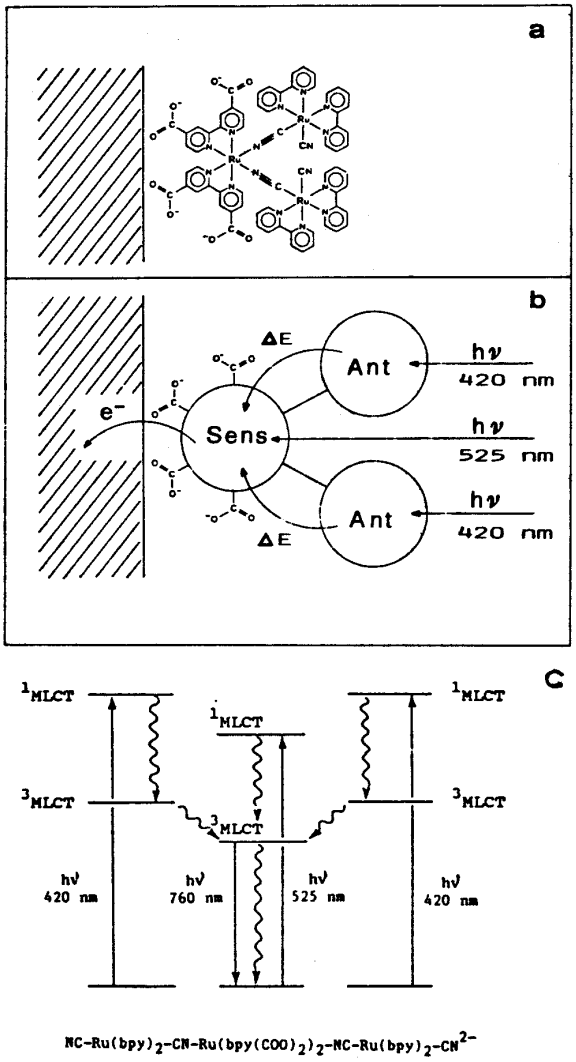

Fig. 17. (a) Schematic representation of the mode attachment of the trinuclear ruthenium complex on the TiO_2 surface. (b) Block diagram showing the function of the trinuclear complex as an antenna-sensitizer molecular device. (c) Qualitative energy level diagram and mechanism of the antenna effect in $[Ru(byp)_2(CN)_2)_2Ru(byp(COO)_2)_2^{2-}$. From [99].

nanocrystalline TiO_2. The 22 Ru(II) nuclear dye with a spherical diameter of 5 nm would obviously be much more severely excluded from the interior TiO_2 nanopores of these electrodes. It is of course possible to increase the pore diameter of transition metal oxides (i.e. 20–100 Å), as has been done by Antonelli and Ying [106] using a ligand assisted micelle template approach, but the effect on light harvesting efficiency and on incident photon to current-collection efficiency (IPCE) with nanoporous TiO_2 sensitized

with multi-nuclear transition metal ligands of varying ''diameter'', has not been reported.

6.1.1.3. Dendritic molecules comprising metal centers of two or more different transition metal ions. Supramolecular systems comprise a vast and ever increasing literature. Less frequently investigated, but of increasing current interest, are supramolecules with multiple metal centers, where metal centers in the same molecule comprise two different metal ions, i.e. Ru(II) and Os(II), as used by Sauvage et al. [107], or three different metals, i.e., Ru(II), Os(II) and Rh(III), as in Balzani et al. [108].

In mononuclear transition metal complexes, synthesis usually follows the following route,

$$M + nL > M(L)_n$$

where M is a metal ion and L is a free ligand. In the more recently introduced synthetic strategy employed by Balzani et al. [108], complexes (building blocks) are used in place of the metal (M) and the ligand (L) in the synthetic reaction given above. Such systems offer the possibility of absorbing light over a broader spectral region than mononuclear metal ligand molecules or the trinuclear Ru(II) ligands described in [99].

As delineated by Balzani et al. [108], ''Each metal containing building block is characterized by its own absorption, luminescence and redox properties. The absorption bands are related to ligand centered (LC, in the UV region) and metal-to ligand charge transfer (MLCT, in the visible region). Luminescence originates from the lowest excited state which is a ^{3}MLCT state, except for the Rh-based cyclometallated units where the lowest state is a ^{3}LC (ligand centered) state. Oxidation is metal centered and reduction is usually ligand centered.''

It is further stated that, ''In the supramolecular structure of the polymetallic species there is a relatively weak electronic interaction among the building blocks which causes (*i*) some shift in the MLCT absorption bands and redox potentials and (*ii*) fast energy transfer from the lowest luminescent level of each unit to the lowest one of the entire supramolecular structure. Luminescence usually originates from such a lowest excited state.''

More recent efforts by Balzani [109] extend the number of different metals and/or ligands that can be incorporated in complexes of high nuclearity. Interesting work along these lines is also described by Rillema [110]. Results from this new strategy should be extremely interesting and may be expected to have great impact on near and long term applications involving the sensitization of nanostructured materials and also in mimicking the photosynthetic process.

6.2. Derivitized Soluble Polymers

Baxter et al. [104] have discussed electron and energy intra strand transfer in polystyrene polymers that contain polypyridyl complexes of Ru(II) or Os(II). Systems of this type are explored as approaches to the creation of molecular level artificial photosynthetic molecular assemblies.

In this approach, a soluble preformed 1:1 copolymer of styrene and chloromethyl styrene is used. These polymer backbones are capable of being derivitized to enable substitution of each chloromethyl group with $[M(bpy)_2(bpyCH_2OH))(PF_6)$, where (M = Ru, Os). The size of the individual complex ($\sim$14 Å) is significantly greater than the repeat distance of the polymeric backbone (5–6 Å). This prevents coiled structures. An average distance of separation between peripheries of adjacent complexes is calculated to be $\sim$7 Å. These heavily loaded polymers were devised to explore their capability of acting as multiple electron oxidants or reductants for potential use in the multielectron reduction of CO_2 or oxidation of H_2O. The high energy content of $CO_2^{\bullet}$ or HO· intermediates, which could result in back reactions with photo-induced M(III) states, makes this a challenging goal. However, it has been determined, with both CW and laser flash experiments, that it is possible to build up multiple oxidative equivalents on single strands of the highly loaded Ru and Os polymers. The ability of this process to occur is attributed to the effect of the Marcus inverted region on the rate of oxidative quenching, where $\Delta G^\circ > \lambda$; ΔG° is the free energy change and λ is the Marcus reorganization energy. Since this reaction is relatively slow, multiple redox equivalents have sufficient time to build up on single polymeric strands.

In this same paper various schemes are discussed in which both Ru(II) and Os(II) ligands are present on the same polymer strand. This was shown to lead to charge carrier migration along the strand. Light absorption characteristics are dominated by the Ru(II) ligands. With high concentrations of an

oxidative quencher present, following excitation of the Ru(II) to Ru(II)*, Ru(III) is formed. Electron transfer from an adjacent Ru(II) moves positive charge along the polymer strand by electron transfer hopping until the Ru(III) is adjacent to an Os(II) ligand. The observed kinetic event is electron transfer from Os(II) to Ru(III) to form Os(III).

The homo polymer of L-glutamic acid (PLGL) is normally in the random coil state at pH 6 in the absence of styrl-7 (S-7), as shown by Jones et al. [111] based on circular dichroism determinations. Self-assembly of the organic dye, S-7, on PLGL in a head to tail dimer configuration, causes the PLGL to retain an increasingly large percentage of the helix configuration as the S-7 dye concentration is increased. The S-7 dimers are believed to be bound to charged sites on the PLGL peptide at regular intervals that depend on the degree of charging of the polymer. The density of the charged dye binding sites can be controlled by variation in pH. At sufficiently low pH, dye can be bound at ''forth residues'', which coincide approximately with the helical turns and would form a regular array of dye dimers on the helix. Similar self assembly characteristics may also apply to other dyes and to metal ligands which could be suitable for electron transfer along the helix at the proper pH.

6.3. *Molecular Assemblies from Dyads to Pentads*

Gust et al. [112] and [113] have provided excellent reviews of research aimed at synthesizing artificial reaction centers that mimic many of the features of naturally occurring photosynthetic reaction centers. A starting point is the porphrin-quinone dyad, with the chemical structure and photochemical pathway that gives rise to a charge separated state, $P^{\bullet+}$-$Q^{\bullet-}$, as shown in Fig. 18. The extension of the lifetime of the charge separated state from a few ps to several hundred ps for dyad structures has been extended into the microsecond domain for triad structures displaying multistep electron transfer, as illustrated in Fig. 19. Triads designed around inorganic chromophores attached to an organic polymer backbone, have already been mentioned in section 6.2. Molecular pentads have been prepared which allow electron and energy pathways that are not consider possible with simpler molecular devices. An example is given in Fig. 20. This molecule is composed of two covalently linked porphyrin moieties. The zinc porphyrin is attached to a carotenoid, and the free base porphyrin to a diquinone with an electron accepting naphthoquinone bonded to an even better electron acceptor, benzoquinone. This molecule exists in an extended form with length of about 80 Å. The final charge separated state has the configuration, $C^{\bullet+}$-P Zn-P-$Q^{\bullet-}$, lifetime of 55 μs, quantum yield 0.83 and preserves approximately one-half of the excitation energy used in its formation.

6.4. *Molecular Devices*

6.4.1. Electronic applications. Charge separated pentads and other similar molecules are capable of producing electrical signals and of integration into electronic devices. Examples being explored include transmembrane electron transfer that utilizes the triad structure of Fig. 21 discussed by [113]. Application of these types of molecules in monolayers, as in Fig. 22; as molecular wires using structures such as that shown in Fig. 20; and as logic elements, and optical switches have been demonstrated.

Exceptional progress has been made in the synthesis of supramolecular systems leading to promising photovoltaic applications. By contrast, incorporation of supramolecules or other large molecules mimicking photosynthesis into electronic devices or logic elements is considered still in its infancy, although a conceptualized very-large-scale-integrated (VLSI) device has been reported by Hopfield et al. [114].

6.4.2. Pseudorotaxanes leading to a molecular abacus. Ballardini et al. [115] and Anelli et al. [116] have devised rotaxanes, which are composed of a macrocyclic ring threaded by a linear component resembling a dumbbell. If one or more of the bulky end groups are absent, the ring can be unthreaded. The resulting supramolecular species is called a pseudo-rotaxane.

A molecular thread, with a 1,5-dioxynaphthalene electron-donating group, when added to a solution containing an electron-accepting cyclophane, threads through the center of the tetra cationic cyclophane producing the 1:1 complex. Light induced unthreading process for the case of a molecular thread consisting of 9-anthracenecarboxylic acid in the presence of a sacrificial reductant has also been discussed. The unthreading can be reversed by allowing oxygen to enter the irradiated solution. A

(a)

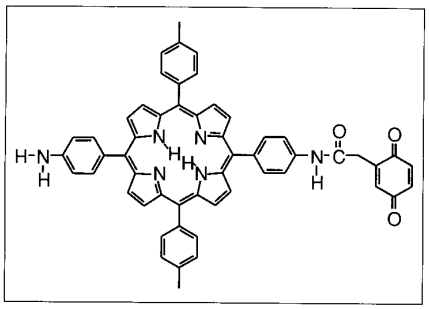

(b)

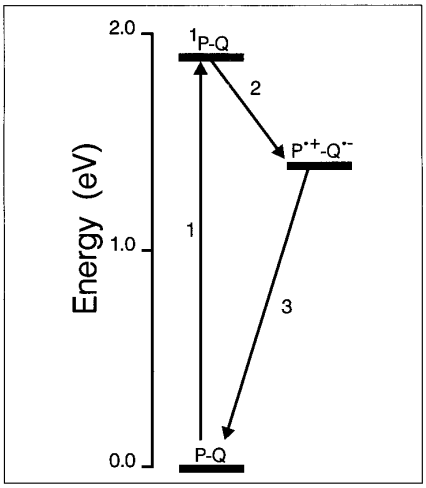

Fig. 18. (a) Structure of porphyrin-quinone dyad consisting of a free base (non-metallated) porphyrin whose first excited singlet state acts as an electron donor to the benzoquinone acceptor moiety. (b) Photochemical pathways for a typical porphyrin-quinone molecular dyad as in (a). The horizontal bars represent the relevant energy states for the molecule, and the arrows indicate interconversion routes. From [112].

(a)

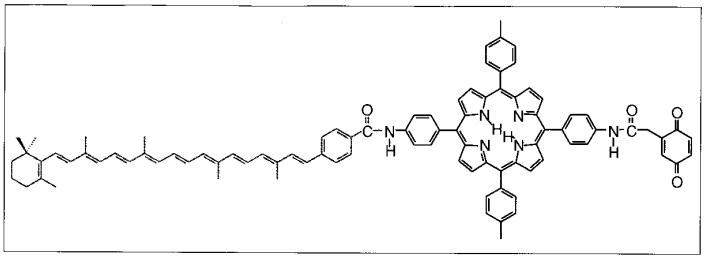

(b)

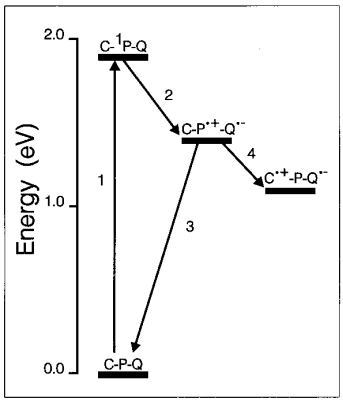

Fig. 19. (a) Structure of carotenoporphyrin-quinone triad. The first excited state of the porphorine donates an electron to the quinone acceptor moiety to yield a C-P$^{\bullet+}$-Q$^{\bullet-}$ charge separated state. Electron transfer from the carotenoid polyene secondary donor to the porphorine radical cation yields the final C$^{\bullet+}$-P-Q$^{\bullet-}$ charge separated state. (b) Photochemical pathways for C-P-Q molecular triad. Step 1 represents excitation of the molecule with light, yielding the first excited singlet state, and the other steps are electron transfer reactions. From [112].

similar principle has been proposed for the creation of molecular shuttles, considered to be equivalent to a molecular abacus.

7. Photochemistry in Organized Molecular Assemblies

7.1. Zeolites

Zeolite cages afford the possibility of carrying out chemical processes within or mediated by reactant molecules or parts of molecules able to enter or be synthesized within these cages. Windows to adjacent cages within the zeolite may restrict entry of molecule D, but allow entry of molecule A. When D and A are confined to adjacent cages, light excitation of D can result in electron transfer to A. Various strategies along these lines are discussed below.

7.1.1. Dye confinement in zeolites. Krueger, Mayer, and Mallouk [117] described a system that combines a zeolite with the dyad structure of Fig. 23, consisting of a ruthenium-based chromophore linked

(a)

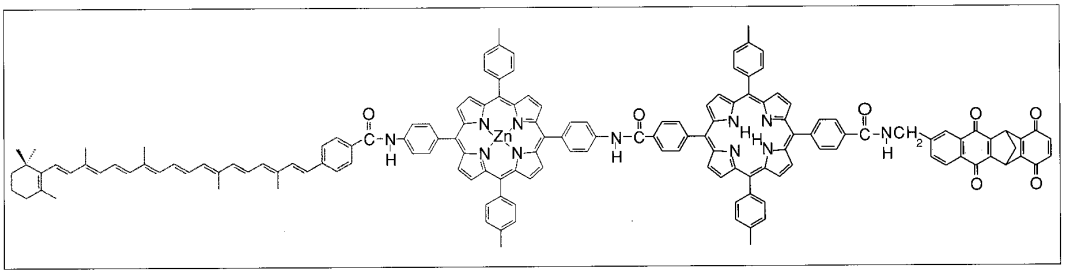

(b)

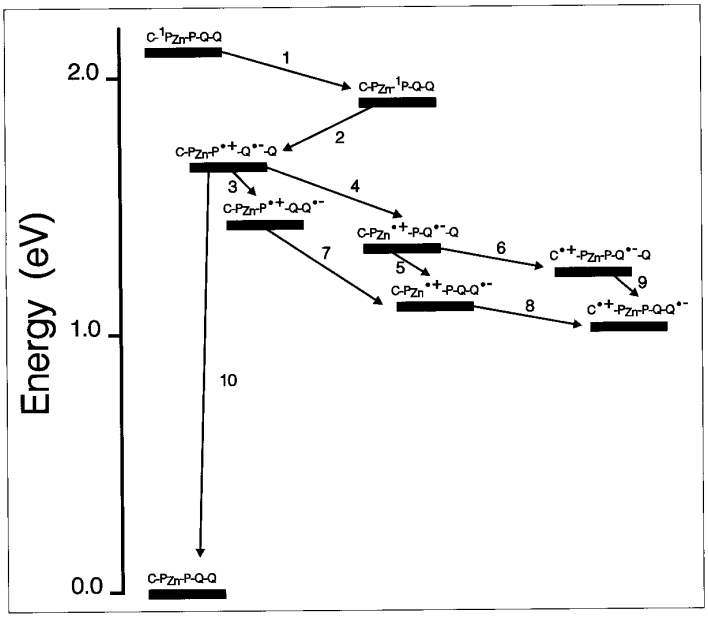

Fig. 20. (a) A pentad artificial photosynthetic reaction center. The central portion of the molecule consists of a zinc porphorine covalently bound to a free base porphorine moiety. The zinc porphorine also bears a caotenoid electron donor, where the free base is linked to a diquinone species consisting of a naphthoquinone bound to a benzoquinone derivative. (b) Photochemical pathways for C-Pzn-P-Q-Q pentad. Step 1 is singlet-singlet energy transfer from the zinc porphorin to the free base. The remaining steps represent electron transfer between the various moieties. From [112].

to an acceptor, which can be represented by RuL_3^{2+}-$2DQ^{2+}$. The DQ^{2+} acceptor moiety is sufficiently small to enter the zeolite L cages, which have undergone prior exchange with benzylviolegen ions, BV^{2+}, while the ruthenium pigment moiety is excluded because of size from entering the zeolite. Excitation of the ruthenium moiety initiates a sequence of electron transfer reactions leading to the formation of the final charge separated state, RuL_3^{3+}-$2DQ^{2+}$-$BV^{\bullet+}$, with lifetime of about 37 ms. A system of this type has been proposed for water splitting.

In another system proposed for water splitting by Ledney et al. [118], a transition metal dye is snythesized within the zeolite cage. The following mechanism for water splitting is considered.

$$D + \text{sunlight} \rightarrow D\cdot$$

$$D\cdot + A \rightarrow D^+ + A^-$$

$$4D^+ + 4OH^- \rightarrow O_2 + 4D + H_2O$$

$$2A^- + 2H^+ \rightarrow H_2 + 2A$$

For this to occur efficiently, back reaction between D^+ and A^- must be prevented and these species must

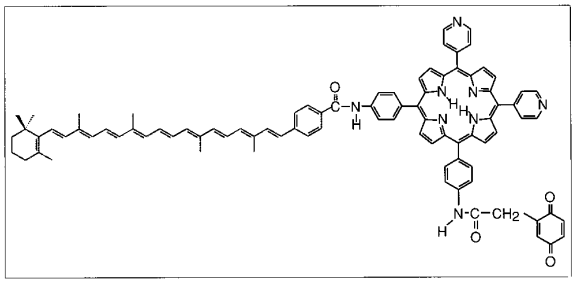

Fig. 21. A carotenoid porphorin quinone triad that functions in a manner similar to that described in Fig. 28, and that carries out photoconduction across a lipid bilayer membrane. From [112].

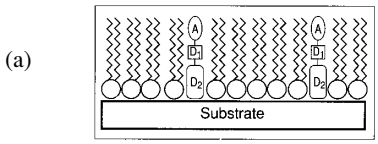

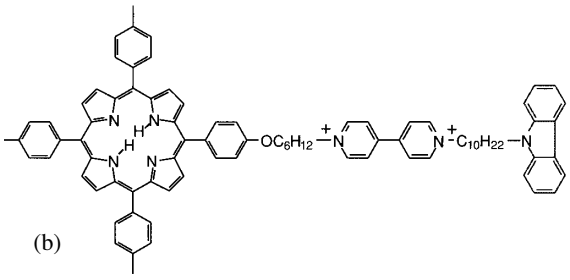

Fig. 22. (a) Schematic representation of a monolayer deposited on a conducting substrate. Photochemically active triad molecules are dispersed in an inert lipid matrix in order to minimize inter molecular interactions within the layer. Excitation of the chromophore D1 would initiate a multistep sequence to yield a $D2^{\cdot+}$-D1-$A^{\cdot-}$ charge-separated state that could interact with electron carriers in the conducting or semiconducting substrate and an aqueous solution on the hydrophobic side of the monolayer to produce an electrical signal. (b) A triad consisting of a viologen moiety bearing both a porphorin primary electron donor and a carbazole secondary donor. This molecule has been used to investigate photoinduced electron transfer in monolayer systems. From Wang, X.D. et al. (1992), as discussed by [112].

be accessible. Zeolite cages have been used as partitioning media for D and A, where D has been $Ru(byp)_3^{2+}$ and A has been viologens.

Zeolite Y consists of 13 Å supercages, separated by

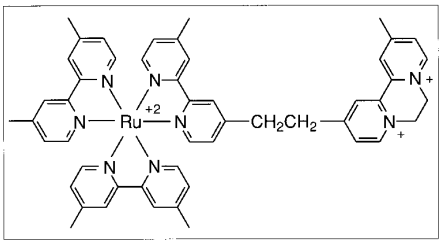

Fig. 23. In this dyad, a ruthenium-based chromophore and primary donor is linked to a primary acceptor, which can enter the pores of a zeolite containing benzylviologen as a secondary acceptor. Excitation of the ruthenium complex leads to reduction of the benzylviologen by a multistep electron transfer sequence. From [112], describing process in [117].

7 Å windows. Therefore $Ru(byp)_3^{2+}$ (12–13 Å) once synthesized within the cage is trapped, but can communicate with other molecules through the 7 Å windows. A system has been formulated consisting of 1 $Ru(byp)_3^{2+}$ per 15 supercages, with the remaining cages occupied by 2 molecules of MV^{2+}. Light excitation produces $Ru(byp)_3^{3+}$ (half-life = 15 μs) and $MV^{+\cdot}$ (stability = hours). Addition of a second neutral viologen, (propylviologen sulfonate, PVS), to the solution phase, which is both too large to enter the zeolite and is energetically positioned to accept electrons from the caged MV^{+}, provides effective charge carrier separation and also ready access of the transfered electron for initiation of chemical reactions. Since electron transfer to PVS takes place at the zeolite surface, synthetic zeolites with mean particle size 200–400 Å were prepared (commercial crystals are >1000 Å). This has the potential of enhancing the product yield. Regeneration of $Ru(byp)_3^{2+}$ from $Ru(byp)_3^{3+}$ remains a slow step limiting O_2 generation. Work is in progress to circumvent this difficulty, i.e., hydration of system with dilute base.

Energy transfer between caged monomer dye molecules in parallel zeolite channels has recently been demonstrated by Binder et al. [119]. It is also shown in a mixture of zeolite microcrystals loaded with pyronine as donor (D) and others loaded with oxonine as acceptor (A), that energy transfer occurs from the D to the A filled zeolite particles.

Monograin layers of zeolite Y encapsulated $Ru(byp)_3^{2+}$ have been prepared on ITO glass by Calzaferri et al. [120], offering a variety of opportunities for solar energy conversion. Feng and Bein [121] have reported the growth of oriented

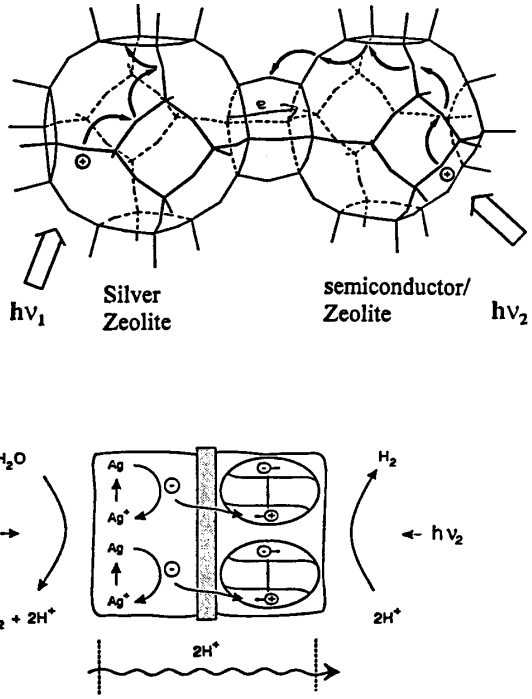

Fig. 24. (a) Accumulation of the photoproduced holes within the zeolite. Hoping from oxygen to oxygen of the zeolite framework is imagined to describe the movement of the holes. Arrangement to couple the oxidative and reductive half-reactions. A zeolite system is used on both sides. A silver zeolite drives the water oxidation. The water reduction is achieved by semiconductor particles encapsulated in a zeolite matrix. From [122].

zincophosphate X crystals on gold surfaces modified with organophosphonate multi-layer films. The channels in these crystals are aligned with [111] surfaces facing in an upward direction with respect to the substrate. References are given in [121] to other work where non-oriented channels have been prepared by depositing or growing crystals on metal or metal oxide supports and in one case to an oriented deposition of a pre-grown crystal by application of an electric field.

7.1.2. Ag-zeolites. Beer, Calzaferri, Li and Waldeck [122] have reported on experiments with Ag-zeolites, where water splitting also constitutes a major objective. The photochemical splitting of water is considered to consist of three parts: the oxidation of water to O_2, reduction of water to H_2 and the coupling of the two processes. The coupling is considered to require a membrane that allows transfer of electrons and protons to the reductive side and prevents recombination.

One embodiment consists of membrane connected zeolites. In the silver zeolite, on the left side of Fig. 24, light is used to catalyze the oxidation of water to form O_2 and H^+ ions. Photoelectrons reduce Ag^+ ions within the zeolite cage and serve as a source of electrons for recombination with holes generated in the semiconductor loaded zeolite on the right side of the membrane. This membrane must also allow transport of H^+ ions from left to right. The primary function of the semiconductor is to provide photoelectrons of suitable energy for reducing H^+ ions to H_2. Recent progress in this area is described in [123].

7.1.3. Hydrocarbon oxidation in zeolite cages with red and near-IR light. In a highly novel and potentially important line of investigation, Frei [124], has demonstrated highly selective oxidation of small alkenes, alkanes, or aromatics when loaded together with O_2 into alkali or alkaline earth exchanged zeolite Y. Within the zeolite cages, a long-lived [(hydrocarbon)$\cdot O_2$] charge transfer state, absorbing in the visible spectral region, is spontaneous formed. Life-times of these species are much shorter in the gas or solution phase. Stabilization of the charge transfer state is attributed to the very high electrostatic field in the zeolite-Y supercage. Irradiation of these bands with red and near IR light results in selective conversion of [(hydrocarbon)$\cdot O_2$] to oxygenated derivatives. Since the ionization potentials of alkenes or substituted benzene increase substantially upon partial oxidation, it is unlikely that secondary oxidation will occur, as is more likely with catalytic autooxidation. This technique has been extended to the use of visible light excitation for the oxidation of other organics confined to the cages of other zeolites, i.e. isobutane $+ O_2$ in zeolite Ba Y, using blue or green light excitation.

7.2. Laminar Systems with Transition Metal Ligands

Layered metal oxide semiconductors of general formula AM_nO_x (A = alkali metal, M = Ti, Nb, Ta), have been prepared by Mallouk et al. [125]. Band gaps are typically 3.3–3.7 eV, making feasible the direct photolysis of water using UV excitation. These materials can be sensitized photolytically with interlaminar Pt deposits and with (RuL_3^{2+} (L = 4, 4′-

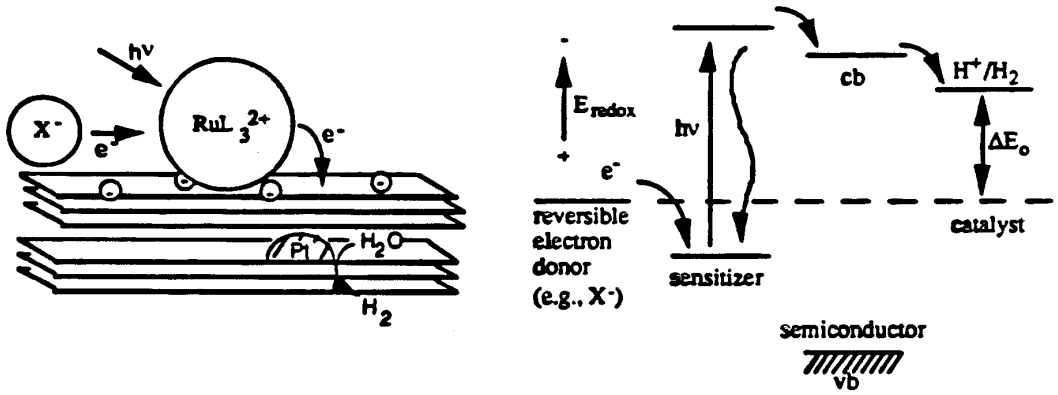

Fig. 25. A layered metal oxide semiconductor spectrally sensitized with a ruthenium complex and derivitized with photolytically deposited Pt. Photosensitized hydrogen evolution has been achieved, which is at present limited in efficiency by back electron transfer by an oxidized donor ion and metal oxide conduction band electrons. New ruthenium complexes are being prepared to block access of the oxidized donor ions with the metal oxide surface as a strategy for increasing efficiency. From [125].

dicarboxy-2,2′-bipyridine)) on the outer surface. I_3^- is used to regenerate the oxidized dye. A schematic diagram is shown in Fig. 25. The quantum efficiency of these systems are presently limited by back electron transfer between the oxidized donor (I_3^{2+}) and metal oxide conduction band electrons. New phosphate and phosphoramidate analogs of RuL_3 have been prepared, with the intent of using these materials both as sensitizing dyes and to block access of the (I_3^{2+}) to the oxide surface, thereby increasing the overall efficiency.

Also described is the delamination of these materials by acid-base reactions, allowing modification in various ways, followed by reassembly to form what have been termed multilayer superlattice structures. An example is a 20 Å layer of a polymer derivitized with RuL_3 sandwiched between 8 Å layers of zirconium phosphate sheets grown on fumed silica. In the presence of an electron donor in solution, excitation at 532 nm yields the oxidized state of the ruthenium dye.

8. Organized Mono- and Multi-layered Molecular Assemblies

Self assembled (SA) monolayers and multilayers consisting of chemisorbed organothiols bonded to Au or Ag, and organosilanes bonded to silica and other substrates have been extensively investigated for a variety of applications, which include thin film optics, sensors, transducers, protective layers, high resolution imaging materials, and functionalized surfaces with specific chemical, biological or adhesive properties, as discussed by Dulcey et al. [126]. Self assembly strategies originating with the Savig group (see [127]) employing linear molecules terminated with a trichlorsilane group at one end and other fuctionalities at the other end have been used by Wasserman et al. [128], to produce SA monolayers and multilayers [129], have been extended by Li et al. [130] to the preparation of chromophoric self-assembled multilayers to form what has been termed an organic superlattice having applications in nonlinear optics.

However, there appear to be relatively few reports that deal with light induced vectorial electron transport and transfer for energy conversion applications, see Christ et al. [131]. The situation is somewhat different in the area of Langmuir-Blodgett (LB) films, according to DeArmond [132], where applications incorporating transition-metal ligands, appear to be an actively emerging area in Japan. The technological importance of chemisorption of thiocarbocyanines and other spectrally sensitizing dyes to form self-assembled structured surface aggregates on the lattice of silver halide particles has been discussed in section 3.2.

In an investigation by the Wrighton group (see [133]), electrodes are potentiostatically derivitized with a redox polymer consisting of a quinone flanked by two benzylviologen subunits, $(BV\text{-}Q\text{-}BV^{6+})_n$. The observed pH-dependent rectification at low coverages was attributed to structural constraints leading to ordered molecular arrays capable of precluding direct electrode access to all the quinone moieties.

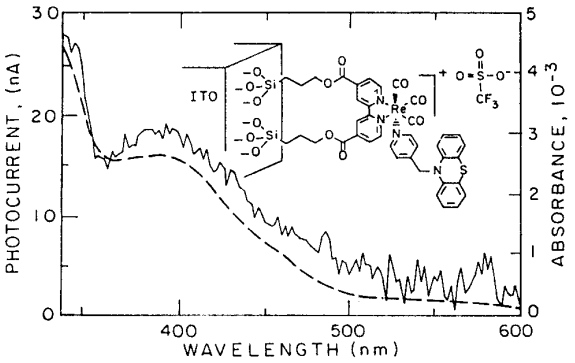

Fig. 26. (a) Comparison of photocurrent versus wavelength data (dashed line) with the absorption spectrum (solid line) of ITO/Re complex. The absorption spectrum correlates directly with the magnitude of the photocurrent. From [131].

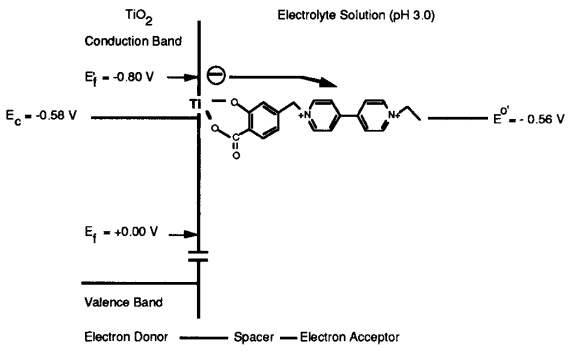

Fig. 27. Heterotriad formed by adsorption at a polycrystalline TiO_2 electrode in an aqueous electrolyte solution. From [134].

8.1. Self-Assembly of Monolayers and Multilayers

Building on the study of Smith et al. [133] demonstrating the importance of physically stable ordered assemblies in attaining vectorially directed charge transport, Christ et al. [131] investigated energy conversion by excited state electron transfer from a multi-functional metal complex covalently linked to an electrode. Attachment of the molecular assemblies to silica gel, glass, and to Pt or ITO electrodes is through -$SiCl_3$ linking groups. Renium carbonyl complexes, together with the sacrificial donor, triethanolamine (TEA), produced sustained photocurrents, as shown in Fig. 26. Electron transfer from pendant PTZ (phenothiazine) to excited Re is found to be approximately 60 times faster than the reverse transfer rate from reduced bipyridine to oxidized PTZ, consistent with Marcus inverted region behavior.

Marguerettaz et al. [134] have combined solid state nanotechnology with supramolecular chemistry to form a heterotriad, consisting of polycrystalline TiO_2 coated on conducting tin oxide glass (fluorine doped), and an adsorbed molecular complex consisting of spacer-acceptor(1)-acceptor(2), as shown in Fig. 27. The spacer moiety of the molecular complex is salicylic acid, which is considered to chemisorb at TiO_2 by chelation to suffice Ti^{4+} atoms. Xenon lamp illumination of the nanostructured TiO_2 heterotriad in an aqueous electrolyte at pH 3.0 leads to spectral changes assigned to electron transfer from the TiO_2 to acceptor(2), with formation of dihydroanthraquinone. Light activated electron transfer to acceptor(1) is not observed in the absence of acceptor(2). Adsorption of transition metal dyes containing carboxylic acid groups to nanostructured TiO_2 has also been effective with transition metal tri-nuclear antenna dyes used in the electrochemical photovoltaic cells applications discussed in section 5.2.

8.1.1. Self-assembled films with semiconductor nano-particles. Kotov, Dékány, and Fendler [135] have used SA techniques to form monolayer films incorporating CdS, PbS or TiO_2 nanoparticles. (They also provide a concise list of references to their own work and of others covering SA and LB investigations relevant to energy conversion and related applications.) Multi-layer deposits of one or more of these semiconducting particulate layers, each separated by a layer of cationic poly(diallylmethylammonium chloride), have been fabricated on metal, glass or plastic. These layered structures, S-$(P/TiO_2)_n$, where S is the substrate, P the polyelectrolite, were demonstrated to be photoconductive, and to increase in conductivity with increasing number of sandwich units ($n = 1$–15). The spontaneous, layer-by-layer self assembly of these nanostructured films is considered to be an example of a membrane-mimetic approach to advanced materials, corresponding to properties of the biological membrane.

8.2. Langmuir-Blodgett Films

LB films containing transition metal complexes is a relatively new and potentially important accomplishment. Sakaguchi et al. [136,137] and Yamada et al. [138] have produced ordered systems of monolayer and multilayer films containing amphiphilic Ru(II) complexes of the 2,2′-bipyridine type having non-

linear optical properties. More recently a prototype diode based on a *p-n* homojunction prepared by a combination of electrochemical cation doping and photochemical anion doping of a polythiophene film spectrally sensitized with $[Ru(bpy)_3]^{2+}$ has been reported [139].

A problem often associated with LB film systems is mechanical and thermal fragility of the monolayer and multilayer films. In SA films, difficulties are centered on the fabrication of multilayer films and incorporation of functional groups. SA films generally have the advantage of higher stability than LB films. Solutions to the LB stability problem are being developed by Bilewicz and Majda [140], using a LB technique to form a SA monolayer. The LB monolayer, formed from a solution containing a thiol, a long chain alcohol and ubiquinone on a gold substrate, is stabilized by the formation of S-Au bonds on the gold substrate. Siloxanes have also been coated by the LB method by Richardson et al. [141] and by Yose et al. [142]. Samha and DeArmond [143] are investigating a promising multilayer hybrid SA-LB film technique incorporating Ru(II) ligand complexes and octadecyltrichlorosilane gel (OTS). Transfer ratios (onto glass microscope slides) near unity derive from the rigidity of the OTS gel of these SA-LB films.

Using SA techniques, Heleg and Willner [144] covalently bound $Si(CH_2)_2$-NH_2 to TiO_2 particles, to which palladium was previously photodeposited. Eosin was then bound to the surface. The resulting photocatalyst was used in the fixation of CO_2-HCO_3^- to formate (HCO_2^-) and H_2 with $\lambda > 435$ nm light.

9. Recommendations

9.1. Short Term Goals

9.1.1. Pollution remediation and electrochemical photovoltaic cells. Evidence is emerging suggesting that heterogeneously catalyzed systems range from those where: *i*. Only the photohole is directly involved in the chemical reaction of interest and the photoelectron must be disposed of in some manner to minimize recombination; *ii*. Both the photoelectron and photohole independently initiate desirable reaction paths, and *iii*. Photoelectrons and photoholes initiate the formation of different intermediates which interact chemically to form either the desired product or a species that will lead to the formation of the desired product. In *i*. and *ii*., charge carrier separation is desirable. In the last case, *iii*., there may be an optimum charge carrier separation distance, where recombination is kept at a tolerable level and reaction rate between the chemical intermediates, initiated by the photo-generated electrons and holes, are in sufficiently close proximity to react at a high rate. Research efforts focusing on the design of heterojunction catalysts to meet the requirements of specific processes are suggested. Among these are:

- Synthesis of transition metal oxide semiconductor particulates and mixed oxides by various techniques such as: *i*. Sol-gel, *ii*. Hydrothermal methods, *iii*. Inert gas condensation followed by controlled oxidation of metal clusters, and *iv*. Fumed oxides as in the Degussa process.
- Control of photoconductor particle size, morphology and porosity (when sintered and as coatings).
- Evaluation of sensitization of porous metal oxides by deposition of narrower band gap inorganic photoconductors within the pores.
- Spectral sensitization by dyes, with increasing attention being given to multi-nuclear transition metal ligands, using metal centers of the same metal or two or more different metals.
- Determination of optimum relationship between sensitizing dye dimensions and pore diameter distribution in nanoporous transition metal oxides used as photocatalysts and photoelectrodes.
- Investigate heterojunction structures to aid in charge carrier separation and as a means of broadening the spectral absorption characteristics to better match the solar spectrum.
- Direct electronic determination of charge carrier dynamics and separation distances in nanostructured photoconducting materials—as an aid in establishing application specific reaction mechanisms (i.e., water splitting, heterogeneous photocatalysis, electrochemical photovoltaics).
- Determination of surface and interparticle band bending in heterojunction photocatalysts and photoelectrodes as related to process efficiency.
- Establish mechanism of photocatalytic oxidative degradation of organic molecules with mixed Ti/Fe oxide photocatalysts, capable of explaining observed maximum in (efficiency vs. % Fe). Is maximum charge carrier separation desirable? Does a Russell type mechanism prevail in which the products of reactions of both photoholes and

photoelectrons lead to the degradation products. Must close proximity of these intermediates on the catalyst surface be balanced against the tendency for electron-hole recombination? This information is expected to be helpful in devising new more effective catalysts, dopants and heterojunction configurations.

- Clarification of the role of intermittent exposure effects in increasing efficiency of heterogeneous photocatalysis leading to the degradation of pollutants [145]. Is the effect the result of decrease in band bending with high intensity CW exposure? In Grätzel cell, is this related to higher IPCE at one sun light intensity compared to higher intensities?
- Determination of energy band structure for nanoporous transition metal oxides in contact with an electrode and spectrally sensitized by transition metal ligands and other dyes. Can spectrally sensitizing dyes adsorbed to nanoporous photoconducting materials be considered to function as Q-sized particles in the same manner as more traditional inorganic semiconducting materials?
- What are the limitations to Grätzel cells? What is the present cost? What is the present lifetime, efficiency etc. and can improvements be expected in the near future, or has optimum theoretical performance been reached? What are the limitations on operating parameters such as light intensity? Can the cell function when oxygen, water and other ambient are present? Has an optimum combination of pore size and ''diameter'' of the sensitizing dye molecule been attained?
- Photocatalytic reactor design should be optimized for specific applications.
- Resolution of the role of ''Hot Electron Injection''.
- Role of ·OH radicals in heterogeneous oxidative degradation of organic pollutants. Are ·OH radicals reacting with organic pollutants on the photocatalyst surface or in the solution phase?
- Role of O_2^- formation in oxidative photocatalysis.

9.1.2. Photocatalytic synthesis. Photocatalytic synthesis appears to be in a very preliminary stage. However, there are several processes having excellent short range possibilities. They are:

- Organic synthesis on nanocrystalline surfaces along the line of Frei [124] in zeolites is still to be investigated. If it works it may have short and long range implications.
- Scale-up of photocatalytic isomerization of 2-butene to produce 1-butene.

9.1.3. Supramolecular systems. There is little question that the synthetic efforts in devising molecular level artificial light harvesting systems has been truly inspiring. Synthetic protocols for producing these molecules are varied and at this stage well understood and controlled. The flexibility of the transition metal systems have been incorporated into the polymer based donor-acceptor (D-A) systems and into linked pentad (D-A) systems. And when we turn to Grätzel Cell applications, the transition metal antenna molecules are contributing significantly by efficiently harvesting light and aiding in vectorially directing photoelectrons to the electrode. Transition metal dyes are also being used as components of D-A charge transfer and charge separation molecules: *i*. To derivatize polymers; *ii*. In linked molecules that have progressed from dyads to pentads, while increasing charge separation distance and lifetime; *iii*. As components of zeolite systems; *iv*. In self-assembled and Langmuir-Blodgett molecular assemblies. Significant progress is anticipated in this area over the next five years, especially as attention is directed to multi-nuclear molecules containing two or more metal atom types, i.e. Ru and Os, etc.

9.1.4. Self-assembled and Langmuir-Blodgett layers. Linking of chromophoric groups into SA and LB mono- and multi-layer assemblies has been demonstrated. One approaches utilizes transition metal complexes in SA layers (see for example [131] and [130]) and in LB layers (see [143]) film structures. Another approach uses alternating polycation and semiconducting nanoparticle layers, each deposited by SA techniques (see [135]). The hybrid SA-LB approach appears to offer great promise, since it is capable of increasing the structural stability of conventional LB layers though the formation of a more rigid gel layer. These techniques merit considerable research effort over the next five years and longer. Some specific examples are:

- SA, LB and SA-LB hybrid techniques focused toward a means of achieving light addressable molecular electronic arrays.

- Monolayer and multilayer films of hydrophobic transition metal complexes that have multielectron charge storage capability as well as redox capability is possible and should be tested in photosynthetic, photodegradation, battery and capacitor applications.
- Luminescence of an ordered array of $[Ru(bpy)_3]^{2+}$ complexes mixed with a fatty acid can lead to optical device applications.
- Electronic diodes prepared from LB layers with transition metal complexes incorporated (see [139]) can be improved by alteration of the film technology and tuning the electron transfer properties of the metal complex—this resulting from the substantial library of Ru(II) diimine complex materials available, according to [132].

9.1.5. Zeolites and lamellar based systems. Zeolites and lamellar systems have the ability to selectively permit or exclude entry of molecular species, depending on cage or lamellar spacing and molecular dimensions. If molecules are synthesized within a zeolite cage, it is possible to immobilize the molecule if its dimensions are larger than those of the cage exit windows. Zeolite cages in which transition metal dyes have been synthesized, or in which they are a component of a donor-acceptor dyad with a benzylviologen threaded into the cage and the metal ligand excluded, have been used in water splitting applications, as have silver halide and other semiconductor filled cages. These approaches merit continued long term effort. There are several novel new approaches suggested for short term (5 year) concentrated evaluation efforts:

- Synthesis of zeolite crystallites of controlled size to better meet the needs of a particular process (see [140]).
- Oriented monolayer growth of zeolites on silicon substrates, with aligned open channels within the crystallites (see [121]).
- Formation of monolayer deposits of densely packed zeolite Y czystallites in which $[Ru(bipy)_3]^{2+}$ is encapsulated (see [120]).
- Lamellar superlattices—investigate photophysical and photochemical properties of superlattices formed by delamination of layered metal oxide semiconductors, derivitization of the separated lamellae with transition metal dyes, and with metallic deposits, followed by reassembly to form the superlattice (see [125]).
- Chemical synthesis of specialty chemicals by light excitation of spontaneously formed (Hydrocarbon$\cdot O_2$) charge-transfer complexes within a zeolite Y cage (see [124]).

9.2. Long Term Goals

9.2.1. Pollution remediation and electrochemical photovoltaic cells.

- Second generation Grätzel cells and photocatalysts other than TiO_2 which absorb a more significant fraction of the solar spectrum.
- Stability of Grätzel cell is a key issue—40 year working lifetime may be required for cost effectiveness. Dye may the biggest problem for long term stability.
- Reproducibility of nanoporous electrode may be a problem.
- Need for fundamental understanding of interaction between molecules and semiconductor electrodes and between semiconductor/liquid junctions.
- Use of liquid junctions may always meet resistance, solid state cell may be required.
- Recombmation is the major bottle neck for photovoltaics. Light induced charge injection is very efficient. However, electric energy conversion is presently $\approx$10%.
- Investigate potential use of nanocrystalline films in photocatalysis, energy storage, batteries, optical switching.
- Photocatalytic degradation of pollutants in air and water is feasible, however, at present one must use UV light. Can efficient, stable, non-contaminating photocatalysts be produced which better match the solar spectrum?

9.2.2. Photocatalytic synthesis. Anpo looks forward to investigation of the photocatalytic reduction of CO_2 with H_2O to produce organic compounds, which he considers to be a worthwhile long range objective. The main problem anticipated involves improvements in efficiency. Almost all photocatalytic systems show high efficiency initially, but loose efficiency with continued use. This is the greatest challenge. He considers that 5–10 years in fundamental research will be necessary, while at the same time developing industrial applications. Perhaps 10 to 20 years will be required to develop an actual operable photocatalytic system. ''The development of environmentally-harmonious industrial process is one of

the most important challenges that should be undertaken and if realized, will become the greatest breakthrough for future generations.''

9.2.3. Supramolecular systems. Balzani [109] has suggested that photochemical splitting of water can be achieved using artificial transition metal antenna molecules for light harvesting and multi-component systems (triads and tetrads) for charge separation. Next step should be the design of catalysts capable of storing electrons or holes in order to convert the one-photon/one electron photo-induced process into a multielectron process. Problems are separation of oxygen from hydrogen and the development of efficient catalysts. In this regard, covalent linking of the transition metal ligands to nanoporous transition metal oxides may be an interesting route for investigation. The Grätzel cell has already produced vectorially directed photoelectron transfer from the antenna molecule to nanoporous TiO_2. Wrighton's group has also demonstrated photoelectron transfer from a transition metal ligand molecule to an ITO electrode, to which it is joined by a self assembly technique through an *n*-pr-$SiCl_3$ linking group. This type of technique may lead the way to molecular device electronics. This could begin to happen within the next 5 years, but it is more likely that it will take closer to 20 years before such devices begin to enter the market place.

9.2.4. Self-assembled and Langmuir-Blodgett layers. New long term opportunities may focus on:

- Less expensive metal complexes such as Cu(II) complexes (square planar) and on Fe(II) octahedral complexes, according to DeArmond.
- Incorporation of nanoparticle semiconductors and metal particles into the LB films containing transition metal complexes have been proposed as new redox and charge storage capability films.
- Scale-up of LB nanometer technology is a likely next step so that results of forefront probe methods can occur i.e., scanning tunneling microscopy (STM), lateral force microscopy (LFM), and scanning tunneling microscopy (STM) has resulted in spectacular achievements including the ability to move individual molecules in a film. Near field microscopy may result in rapid development since commercial instruments have already been developed. These techniques provide the ability to distinguish between functional groups of individual molecules and the possibility to store (WRITE) and retrieve (READ) immense amounts of information from solid LB films and also SA layers.

9.2.5. Zeolites and lamellar based systems. Each of the suggestions mentioned above as short term goals in this area should also be considered as meriting long term investigation. The two listed below are mentioned for special consideration.

- Water splitting using zeolites continues to be attractive. It is one of the few approaches where there appears to be a clear means of compartmentalizing formation of O_2 and H_2.
- Chemical synthesis by light excitation of (Hydrocarbon·O_2) charge-transfer complex.

Acknowledgment

I would like to take this opportunity to express my appreciation to the many respondents to the questionnaire on research needs. This input, which in many cases was of considerable depth, was very helpful. Special thanks is extended to Nick Serpone for his lecture, ''Photochemistry of Nanostructured Materials'', on December 2, 1994 at the *DOE Workshop on Energy Applications of Nanofabricated Materials*, organized by the Energy Laboratory of Massachusetts Institute of Technology, Cambridge, MA and for his generosity in making his notes and reference materials available during the preparation of this chapter.

References

1. E.K. Wilson, ''Zero-Valent Metals Provide Possible Solution To Groundwater Problems'', *Chemical and Engineering News* **July 3**, p. 19 (1995).
2. F.W. Wilkins and D.M. Blake, ''Use Solar Energy to Drive Chemical Processes'', *Chemical Engineering Progress*, **June**, p. 41 (1994).
3. M.K. Nazeeruddin, A. Kay, I. Rodicio, R. Humphrey-Baker, E. Muller, P. Liska, N. Vlachopoulos, and M. Grätzel, *J. Am. Chem. Soc.*, **115**, 6382 (1993).
4. B. Levy, ''Photocatalytic and photographic heterojunctions,'' in *Photochem. Conv. Storage of Solar Energy*; eds. E. Pelizzetti and M. Schiavello, Kluwer Acad. Pub., 1991, p. 337 (1991).
5. H. Tributsch, *Solar Energy Materials and Solar Cells*, **31**, 548 (1994).
6. V. Balzani, *Supramolecular Photochemistry* (Reidel

Publishing Co., 1987).
7. M.G. Bawendi, ''Synthesis and Spectroscopy of II-VI Quantum Dots: An Overview,'' *Confined Electrons and Photons*, edited by E. Burstein and C. Weisbuch, Plenum Press, NY, p. 339, 1995.
8. D.M. Blake, ''Bibliography of Work on the Photocatalytic Removal of Hazardous Compounds from Water and Air'' (1994).
9. D.M. Blake, ''Solar Photochemistry-Twenty Years of Progress, What's Been Accomplished, and Where Does It Lead'', NREL/TP-430-6084, DE94006906 (1995).
10. M. Grätzel, *Heterogeneous Photochemical Electron Transfer* (CRC Press, Boca Raton, FL, 1989).
11. A. Henglein, *Topics in Current Chemistry*, **143**, 113 (1988).
12. P.V. Kamat, *Prog. Reaction Kinetics*, **19**, 277 (1994).
13. N.S. Lewis, *Accounts Chem. Res.*, **41**, 21 (1990).
14. R. Memming, ''Photoelectrochemical utilization of solar energy,'' in *Photochemistry and Photophysics*, **vol. II**, ed. J.F. Rabek, CRC Press, Boca Raton, FL, p. 143, (1990).
15. A.J. Nozic, ''Size quantization effects in photocatalysis'', in *Photocatalytic Purification and Treatment of Water and Air*, eds. D.F. Ollis, and H. Al-Ekabi, p. 39 (1993).
16. A.J. Nozic, *Sol. Energ. Mat. Sol. Cells*, **38**, 327 (1995).
17. N. Serpone, E. Pelizzetti, *Photocatalysis: Fundamentals and Applications* (Wiley, New York, 1989).
18. N. Serpone, R. Terzian, D. Lawless, and J.-M. Herrmann, in *Advances in Electron Transfer Chemistry*, **3**, 33 (1993).
19. M.L. Steigewald and L.E. Brus, *Acc. Chem. Res.* **23**, 183 (1990).
20. H. Tributsch, ''Photoelectrocatalysis'', in *Photocatalysis: Fundamentals and Applications*, eds., N. Serpone and E. Pelizzetti, Wiley, New York, p. 339 (1989).
21. A.J. Nozic and S.E. Ronco, eds. (1996) ''Research Opportunities in Photochemical Sciences'', DOE/BES Workshop, February 5–8, Estes Park, CO. Available on Internet at: http://www.er.doe.gov.production/bes/chm/photochem/wkshop.html
22. A. Fujishima and K. Honda, *Nature*, **238**, 37 (1972).
23. J. Bardeen, ''Semiconductor Research Leading to the Point Contact Transistor,'' Nobel Prize in Physics Award Address, Elsevier Publishing Co. 1956.
24. Y. Nakato and H. Tsubomura, *J. Photochemistry*, **29**, 257 (1985).
25. Y. Nakato, H. Yano, S. Nishiura, T. Ueda, and H. Tsubomura, *J. Electroanal. Chem.*, **228**, 97 (1987).
26. A. Heller, Y. Degani, D.W. Johnson, and P.K. Gallagher, *J. Phys. Chem.*, **91**, 5987 (1987).
27. M. Grätzel, ''Vectorial Electron Transfer in Organized Assemblies and Colloidal Semiconductors'' in *Supramolecular Photochemistry*, edited by V. Balzani, Reidel Publ. Co., Dordrect, 435 (1987).
28. C.R. Dickson and B. Levy, *J. Photogr. Sci. Eng.*, **18**, 524 (1974).
29. Y. Wang and N. Heron, *J. Phys. Chem.*, **95**, 525 (1991).
30. T.-G. Zhang and B. Levy, ''Field assisted charge transport in dye sensitized AgX and Pt-TiO_2-Dye particulate heterojunctions'', in *Proceedings of the International Conference of Photographic Science (ICPS'94)*, May 15–20, Rochester, New York.
31. K. Takahasi and M. Konagai, *Amorphous Silicon Solar Cells* (John Wiley and Sons, NY, 124, 1986).
32. C. Zou, M.R.V. Sahyun, M.E. Mueller, B. Levy, and T.-G. Zhang, *J. Imag. Sci. Tech.*, **39**, 106 (1995).
33. J. Schwitzgebel, J.G. Ekerdt, H. Gerischer, and A. Heller, *J. Phys. Chem.*, **99**, 5633 (1995).
34. D.W. Bahnemann, *Israel J. Chem.*, **33**, 115 (1993).
35. M. Sadeghi, W. Liu, T.-G. Zhang, P. Stavropoulos, and B. Levy, *Journal of Physical Chemistry*, **100**, 19466 (1996).
36. B. Levy, *Photogr. Sci. Eng.*, **15**, 279 (1971).
37. H. Gerisher, ''Conditions for an efficient photocatalytic activity of TiO_2 particles'', in *Photocatalytic Purification and Treatment of Water and Air*, eds. D.F. Ollis and H. Al-Ekabi (Elsevier Science Publishers B. V., 1, 1993).
38. N.N. Lichtin and M. Avudaithai, *Res. Chem. Intermed.*, **20**, 755 (1994).
39. G.B. Raupp and L.A. Dibble, ''Solid Photocatalytic Oxidation of Environmental Pollutants,'' *U.S. Patent No. 5,045,288*, Sept. 15 (1991).
40. N.N. Lichtin, J. Dong, and K.M. Vijayakumar, *Water Poll Res. J. Canada*, **27**, 203 (1992).
41. C.R. Berry, *Phys. Rev.*, **153**, 989 (1967).
42. B. Levy, W. Liu, and E.S. Gilbert, *J. Phys. Chem.*, **101**, 1810 (1997).
43. W. West, ''The Spectral Sensitivity of Emulsions, Spectral Sensitization, Desensitization and Other Photographic Effects of Dyes'', in *Neblette's Handbook of Photography and Reprography*, 7th edition, ed. J.M. Sturge (Van Nostrand Reinhold Co., p. 87, 1977).
44. B. Levy and N. Mattucci, *Photgr. Sci. Eng.*, **14**, 308 (1970).
45. K. Norland, A. Ames, and T. Taylor, *Photogr. Sci. Eng.*, **14**, 295 (1970).
46. T.-G. Zhang and B. Levy, ''Modulation of photocharge polarity by light intensity in optically formed oriented AgX/Ag heterojunction arrays'', *Bulgarian Chemical Communications*, **26(3/4)**, 412 (1993).
47. H.W. Vogel, (1874) letter written to The Philadelphia Photographer, **11**, p. 25; reprinted *Photogr. Sci. Engr.*, **18**, p. 33 (1974).
48. M.P. Lippmann, ''La photographie des couleurs,'' *Comptes Rendus Hebdomadaires des Seances de l'Academie des Sciences*, **112**, p. 274. (see also Bjelkhagen, H.I. (1995) ''Silver-Halide Recording Materials for Holography and Their Processing,'' Springer, Berlin, pp. 4–5, 14) (1891).
49. B. Levy, *Photogr. Sci. Eng.*, **27**, 204 (1983).
50. J. Maskasky, *Photogr. Sci. Engr.*, **25**, 96 (1981).
51. T. Sugimoto and K. Miyake, *J. Coll. and Interface Sci.*, **140**, 348 (1990).
52. T. Takizawa, T. Watanabe, and K. Honda, *J. Phys. Chem.*, **82**, 1391 (1978).
53. ibid., **84**, 51 (1980).
54. T. Watanabe, T. Takizawa, and K. Honda, *Ber. Bunsenges. Phys. Chem.*, **85**, 430 (1981).
55. P.V. Kamat and N.M. Dimitrijevic, *Sol. Energy*, **44**, 83 (1990).
56. T. Sakata, ''Heterogeneous Photocatalysis at Liquid-Solid Interfaces'', in *Photocatalysis: Fundamentals and Applications*, eds. N. Serpone and E. Pelizzetti (Wiley, New York 311, 1989).
57. N. Serpone, P. Pichat, J.M. Herrmann, and E. Pelizzetti,

''Inter-Particle Electron Transfer in Semiconductor Dispersions: A New Strategy in Photocatalysis'', in *Supramolecular Photochemistry*, ed., V. Balzani, Reidel Publishing Co. p. 415 (1987).
58. A. Sobcyznski, A.J. Bard, A. Champion, M.A. Fox, T. Mallouk, S.E. Webber, and J.M. White, *J. Phys. Chem.*, **91**, 3316 (1987).
59. V.N. Parmon and K.I. Zamaraev, ''Catalysis in Conversion and Storage of Solar Energy: Photocatalysis Versus Thermocatalysis. Advances and Unsolved Problems'', in *Photochemical Energy Conversion—Proceedings of the Seventh International Conference on Photochemical Conversion and Storage of Solar Energy*, July 31–August 5, 1988, eds. J.R. Norris and D. Meisel, Elsevier, NY, 1989, p. 330, (1988).
60. V.N. Parmon and K.I. Zamaraev, ''Homogeneous and Heterogeneous Catalytic Systems for Conversion and Storage of Solar Energy'', *Proceedings of the Eighth International Conference on Photochemical Conversion and Storage of Solar Energy*, July 15–20, 1990, eds., E. Pelizzetti and M. Schiavello, Kluwer Acad. Publ., Dordrect, 1991, p. 412, (1990).
61. H. Gerisher and M. Lubke, *J. Electroanal. Chem.*, **204**, 225 (1986).
62. L. Spanhel, H. Weller, and A. Henglein, *J. Am. Chem. Soc.*, **109**, 6632 (1987).
63. A. Henglein, M. Gutierrez, H. Weller, A. Fojtik, and A. Jirkovsky, *Ber. Bunsenges. Phys. Chem.*, **93**, 593 (1989).
64. H.S. Zhou, I. Honma, H. Komiyama, and J.W. Haus, *J. Phys. Chem.*, **97**, 895 (1993).
65. E.P. Davey and E.B. Knott, ''Photographic AgBr Emulsion Containing Some AgI,'' U.S. Pat. 2,592,250, April 8 (1952).
66. B. Zuckerman, *Photogr. Sci. Eng.*, **20**, 111 (1976).
67. A. Mews, A. Eychmuller, M. Giersig, D. Schoss, and H. Weller, *J. Phys. Chem.*, **98**, 934 (1994).
68. D. Fitzmaurice, H. Frei, and J. Rabani, *J. Phys. Chem.*, **99**, 9176 (1995).
69. J. Rabani, *J. Phys. Chem.*, **93**, 7707 (1989).
70. P.K. Gopidas, M. Bohorquez, and P.V. Kamat, *J. Phys. Chem.*, **94**, 6435 (1990).
71. I. Bedja and P.V. Kamat, *J. Phys. Chem.*, **99**, 9182 (1995).
72. P. Lawless, S. Kapor, and D. Meisel, *J. Phys. Chem.*, **99**[25], 10329 (1995).
73. H. Kobayashi, F. Mizuno, Y. Nakato, and H. Tsubomura, *J. Phys. Chem.*, **95**, 819 (1991).
74. W. Choi, A. Termin, and M.R. Hoffmann, *J. Phys. Chem.*, **98**, 13669 (1994).
75. S.T. Martin, C.L. Morrison, and M.R. Hoffmann, *J. Phys. Chem.*, **98**, 13695 (1994).
76. L.M. Kellogg, *Photogr. Sci. Eng.*, **18**, 378 (1974).
77. M.A. Anderson, S. Yamazaki-Nishida, and S. Cervera-Marrch, in *Photocatalytic Purification and Treatment of Water and Air*, ed. D. Ollis and D.F. Al-Ekabi, Elsevier Science Publishers, New York (1993).
78. B. O'Regan and M. Grätzel, *Nature*, **353**, 737 (1991).
79. E. Pelizzetti, C. Minero, E. Borgarello, L. Tinucci, and N. Serpone, *Langmuir*, **9**, 2995 (1993).
80. N.N. Lichtin and M. Avudiathia, private communication (1994).
81. A. Yasumori, K. Yamazaki, S. Shibata, and M. Yamane, *J. Ceramic Soc. Japan*, **102**, 702 (1994).
82. C. Anderson and A.J. Bard, *J. Phys. Chem.*, **99**, 9882 (1995).
83. C. Bonner, S. Diol, C.A. Schuttenmaer, J. Cao, Y.L. Gao, and R.J.D. Miller, *Sol. Energ. Mat. Sol. Cells*, **38**, 331 (1995).
84. N.S. Lewis, *Sol. Energ. Mat. Sol. Cells*, **38**, 323 (1995).
85. J-E. Moser, *Sol. Energ. Mat. Sol. Cells*, **38**, 343 (1995).
86. H. Tributsch and F. Willig, *Sol. Energ. Mat. Sol. Cells*, **38**, 355 (1995).
87. A. Hagfeldt, N. Vlachopoulos, and M. Grätzel, *J. Electrochem. Soc.*, in press.
88. H.M. Lin, C.M. Hsu, H.Y. Yang, P.Y. Leeb, and C.C. Yang, *Sensors and Actuators B-Chemical*, **22**, 63 (1994).
89. G. Smestad, ''The Grätzel Cell: A Solar Cell Based on Photosynthesis and Photography,'' *The Spectrum*, published by Bowling Green University, Bowling Green, Ohio, **7(2)**, p. 16 (1994).
90. P. Hoyer, R. Eichberger, and H. Weller, *Ber. Bunsenges. Phys. Chem.*, **97**, 630 (and refs. therein) (1993).
91. L. Kavan, T. Stoto, M. Grätzel, D. Fitzmaurice, and V. Shklover, *J. Phys. Chem.*, **97**, 9493 (1993).
92. B. Levy, W. Liu, and E.S. Gilbert, ''Directed Photocurrents in Nanostructured $SnO_2/TiO_2/Ru(II)L_2(CNS)_2$ Hetero-junctions'', in *Fine Particles Science and Technology from Micro to Nanoparticles*, Proceedings of NATO Advanced Research Workshop, Acquafredda di Maratea, Italy, July 15-21, 1955, ed. Ezio Pelizzetti, Kluwer Academic Publishers, pp. 343–370.
93. S. Gilbert, unpublished results (1994).
94. K. Schwarzburg and F. Willig, *Applied Phys. Lett.*, **58**, 2520 (1991).
95. R. Könenkamp, R. Henninger, and P. Hoyer, *J. Phys. Chem.*, **97**, 7328–7330 (1993).
96. R. Könenkamp and R. Henninger, *Applied Physics*, **A58**, 87 (1994).
97. A. Hagfeldt, U. Bjorksten, and S.E. Lindquist, *Sol. Energy Mat., Sol. Cells*, **27**, 293 (1992).
98. S. Sodergren, A. Hagfeldt, J. Olsson, and S.-E. Lindquist, *J. Phys. Chem.*, **98**, 5552 (1994).
99. R. Amadelli, R. Argazzi, A. Bibnozzi and F. Scandola, *J. Am. Chem. Soc.*, **112**, 7099 (1990).
100. R. Bube, *Photoelectronic Properties of Semiconductors*, Cambridge University Press, Cambridge, Great Britain, Ch. 12, pp. 280–305 (1992).
101. M. Sadeghi, private communication (1995).
102. S. Gilbert, private communication (1995).
103. R. Vogel, P. Hoyer, and H. Weller, *J. Chem. Phys.*, **98**, 3183 (1994).
104. S.M. Baxter, W.E. Jones, E. Danielson, L. Worl, G. Strouse, J. Younathan, and T.J. Meyer, *Coordination Chemistry Reviews*, **111**, 47 (1991).
105. S. Serroni, G. Denti, S. Campagna, A. Juris, and V. Balzani, *Angew. Chem. Int. Ed. Engl.*, **31(10)**, 1493 (1992).
106. D.M. Antonelli and J.Y. Ying, *Angew. Chem. Int. Ed. Engl.*, **34**, 18, 2014 (1995).
107. H.-P. Sauvage, J.-C. Collin, J.-C. Chambron, S. Guillerez, and C. Coudret, *Chem. Rev.*, **94**, 993 (1994).
108. V. Balzani, S. Campagna, G. Denti, A. Juris, S. Serroni, and M. Venturi, *Coordination Chemistry Reviews*, **132**, 1 (1994).

109. V. Balzani, *Proc. 19th DOE Solar Photochem. Res. Conf.*, 1 (1995).
110. D.P. Rillema, *Proc. 19th DOE Solar Photochem. Res. Conf.*, p. 3 (1995).
111. G. Jones, C. Oh, and G.L. Indig, ''Organic Dyes Bound to Polyelectrolytes: Photophysical Probes of Binding Domains and Biopolymer Conformation,'' in *Aquatic and Surface Photochemistry*, eds. G.R. Helz, R.G. Zepp, and D.G. Crosby (Lewis Publishers, Boca Raton, p. 129, 1994).
112. D. Gust, T.A. Moore, and A.L. Moore, *Accounts of Chemical Research*, **26**, p. 198 (1993).
113. D. Gust, T.A. Moore, and A.L. Moore, *IEEE Engineering in Medicine and Biology*, Feb./Mar., 58 (1994).
114. J.J. Hopfield, J.N. Onuchic, and D.N. Bertan, *J. Phys. Chem.*, **93**, 6350 (1989).
115. R. Ballardini, V. Balzani, M.T. Gandolfi, L. Prodi, M. Venturi, D. Philp, H.G. Ricketts, and J.F. Stoddari, *Angew. Chem. Int. Ed. Engl.*, **32**, 1301 (1993).
116. P.L. Anelli, P.R. Ashton, R. Ballardini, V. Balzani, M. Delgado, M.T. Gandolfi, T.T. Goodnow, A.E. Kaifer, D. Philip, M. Pietraszkiewicz, L. Prodi, M.V. Reddington, A.M.Z. Slawin, N. Spencer, J.F. Stoddart, C. Vicent, and D.J. Williams, *J. Am. Chem. Soc.*, **114**, 193 (1992).
117. J.S. Krueger, J.E. Mayer, and T.E. Mallouk, *J. Am. Chem. Soc.*, **110**, 8232 (1988).
118. M.B. Ledney and P.K. Dutta, ''Strategies for Efficient Production and Access to Photochemically Generated Redox Species in Zeolites,'' in *Tenth Int. Conf. on PhotoChemical Conversion and Storage of Solar Energy (IPS-10)*, ed. G. Calzaferri, Interlaken, Switzerland, p. 21 (1994).
119. F. Binder, G. Calzaferri, and N. Gfeller, *Solar Energy Materials and Solar Cells*, **38**, 175 (1995).
120. G. Calzaferri, A. Kunzmann, and J. Li, ''Photophysical and Photoelectrochemical Properties of $Ru(byp)_3^{2+}$ Encapsulated in Zeolite Y,'' in *Tenth Int. Conf. on PhotoChemical Conversion and Storage of Solar Energy (IPS-10)*, edited by G. Calzaferri, Interlaken, Switzerland, p. 455 (1994).
121. S. Feng and T. Bein, *Nature*, **386**, 834 (1994).
122. R. Beer, G. Calzaferri, J. Li, and B. Waldeck, *Coordination Chemistry Reviews*, **111**, 193 (1991).
123. *Tenth Int. Conf. on PhotoChemical Conversion and Storage of Solar Energy (IPS-10)*, ed. G. Calzaferri, Interlaken, Switzerland (1994).
124. H. Frei, *Proc. 19th DOE Solar Photochem. Res. Conf.*, 18 (1995).
125. T.E. Mallouk, S.W. Keller, G.B. Saupe, and S.A. Johnson, *Proc. 19th DOE Solar Photochem. Res. Conf.*, 21 (1995).
126. C.S. Dulcey, J.H. Georger, Jr., V. Krauthamer, D.A. Stenger, T.L. Fare, and J.M. Calvert, *Science*, **252**, 551 (1991).
127. M. Pomerantz, A. Segmuller, L. Netzer, and J. Savig, *J. Thin Solid Films*, **132**, 153 (1985).
128. S.R. Wasserman, Y.-T. Tao, and G.M. Whitesides, *Langmuir*, **5**, 1074 (1989).
129. N. Tillman, A. Ullman, and T.L. Penner, *Langmuir*, **5**, 101 (1989).
130. D.-Q. Li, M.A. Ratner, and T.J. Marks, *J. Am. Chem. Soc.*, **112**, 7389 (1990).
131. C.S. Christ, J. Yu, X. Zhao, G.T.R. Palmore, and M. Wrighton, *Inorg. Chem.*, **31**, 4439 (1992).
132. M.K. DeArmond, private communication, October 12, 1995.
133. D.K. Smith, G.A. Lane, and M.S. Wrighton, *J. Phys. Chem.*, **92**, 2616 (1988).
134. X. Marguerettaz, S.N. Rao, R. Redmond, and D. Fitzmaurice, ''Heterosupramolecular Chemistry: Long-lived light-induced charge separation by vectorial electron flow in a heterotriad,'' in *Optical materials Technology for Energy Efficiency and Solar Energy Conversion XIII SPIE Proceedings*, **Vol. 2255**, p. 793 (1994).
135. N.A. Kotov, I. Dékány, and J.H. Fendler, *J. Phys. Chem.*, **99**, 13065 (1995).
136. H. Sakaguchi, T. Nakamura, T. Nagamura, T. Ogawa, and T. Matsuo, *Chem. Letters*, 1715 (1989).
137. H. Sakaguchi, T. Nagamura, and T. Matsuo, *Applied Organometallic Chemistry*, **5**, 257 (1991).
138. S. Yamada, T. Nakano, and T. Matsuo, *Thin Solid Films*, **245**, 196 (1994).
139. Y. Kunugi, Y. Harima, and K. Yamashita, *J. Chem. Soc. Chemical Communications*, no. 7, April, 787 (1995).
140. R. Bilewicz and M. Majda, *Langmuir*, **7**, 2794 (1991).
141. T. Richardson, G.G. Roberts, S. Holder, and D. Lacy, *Thin Solid Films*, **210/211**, 299 (1992).
142. K. Yase, S. Schwiegk, G. Lieser, and G. Wegner, *Thin Solid Films*, **130**, 213 (1992).
143. H. Samha and M.K. DeArmond, *Langmuir*, **9**, 1927 (1993).
144. V. Heleg and I. Willner, *J. Chem. Soc.*, *Chem. Commun.*, p. 2113 (1994)
145. J.G. Sczechowski, C.A. Koval, and R.D. Noble, ''Improved photoefficiencies for TiO_2 photocatalytic reactors through the use of controlled periodic illumination'', in *Photocatalytic Purification and Treatment of Water and Air*, eds. D.F. Ollis and H. Al-Ekabi, Elsevier, Amsterdam, (1993).